

Quantum Wave Atom Transforms

Marianna Podzorova^{1,3} and Yi-Kai Liu^{2,3}

¹Department of Computer Science, University of Maryland, College Park, MD

²Applied and Computational Mathematics Division, National Institute of Standards and Technology (NIST), Gaithersburg, MD

³Joint Center for Quantum Information and Computer Science (QuICS), NIST/University of Maryland, College Park, MD

Abstract

This paper constructs the first quantum algorithm for wavelet packet transforms with a tree structure, sometimes called wave atom transforms. Classically, wave atoms are used to construct sparse representations of differential operators, which enable fast numerical algorithms for partial differential equations. Compared to previous work, our quantum algorithm can implement a larger class of wavelet and wave atom transforms, by using an efficient representation for a larger class of possible tree structures. Our quantum implementation has $O(\text{poly}(n))$ gate complexity for the transform of dimension 2^n , while classical implementations have $O(n2^n)$ floating point operations. The result can be used to improve existing quantum algorithms for solving hyperbolic partial differential equations.

1 Introduction

The quantum Fourier transform plays an important role in many quantum algorithms that achieve an exponential speedup over classical algorithms [1, 2]. However, less is known about the potential utility of quantum wavelet transforms.

In classical signal processing, wavelets are a powerful tool for constructing sparse representations of complicated signals, using specially-tailored basis functions that are well-concentrated in both time and frequency. This has motivated the study of a vast variety of different wavelet families, characterized by various choices of vanishing moments, size of wave packet support, symmetry, smoothness, and other elements of mathematical design: Shannon, Meyer, Haar, Battle-Lemarié, or Daubechies compactly supported wavelets [3, 4], Coiflets [5], Ricker hats [6], Gabor atoms [7], wave atoms [8–11], and curvelets [8, 12].

Among these families of wavelets, wave atoms and curvelets are known to provide especially *sparse* representations for certain differential operators that arise in the study of wave equations [8, 10–13]. This allows their application as a potentially effective preconditioner for partial differential equations [8, 14]. So, some wave packet bases can be valuable for creating sparse representations of linear operators.

This is potentially beneficial for quantum algorithms, for the following reason: Quantum algorithms, such as Harrow-Hassidim-Lloyd [15, 16], can in principle solve a linear system of equations $Ax = b$ in dimension N , with running time that scales polylogarithmically with N — an exponential speedup over classical algorithms. (A large body of work has shown similar speedups for solving differential equations, and simulating Hamiltonian time evolution; see, e.g., [17–19].) But this result holds only under strong assumptions: in addition to being well-conditioned, the linear system must have an extremely compact description, which is efficiently computable, using space and time polylogarithmic in N . Furthermore, there must be ways to prepare the quantum state that encodes b , and read out interesting properties of the solution x , which are similarly efficient (i.e., running in time polylogarithmic in N). Satisfying these assumptions, in order to make use of these algorithms, is a daunting challenge.

Unsurprisingly, there has been growing interest in developing techniques for solving the above problems (namely, efficient representation of linear operators, state preparation, and readout). Notable progress has been made, particularly using techniques that involve sparsity [20, 21]. This leads us to ask two natural questions: (1) Can wavelet transforms be implemented efficiently (with running time polylogarithmic in the dimension N) on a quantum computer? (2) Can these wavelet transforms be used to construct sparse representations, and perform efficient state preparation and readout, in order to achieve exponential quantum speedups?

In this paper, we address question (1), by describing efficient quantum circuits for implementing wave atom transforms that are characterized by wave packet trees [4]. Our main contribution, compared to recent work on this topic [22], is to handle a large class of wave packet trees. This allows us to use wave packets that obey a so-called “parabolic” scaling law, where the wavelength (of each wave packet) is proportional to the square of the diameter (of the set on which the wave packet is supported). This scaling behavior is crucial for constructing sparse representations of linear operators that appear, e.g., in solving wave equations [9]. This suggests that our quantum wave atom transform will be useful for addressing question (2) above. In particular, our techniques suggest a new approach to solving wave equations on a quantum computer, potentially improving on existing methods [23].

Our results can also be compared to previous implementations of quantum wavelet transforms [24–30], as well as other quantum algorithms that use wavelets to solve differential equations [31, 32] and other more exotic problems [33, 34].

2 Preliminaries

2.1 Notations and assumptions

A universal gate set, such as Clifford+ T , enables the approximation of any unitary transformation with arbitrary precision ε [35, 36]. In analyzing gate complexity, this

Fig. 1 Circuit representations of standard quantum gates. Left column (from top to bottom): phase shift P_k -, X -, Z - and H -gates.

Center-top: SWAP gate.

Center-bottom: controlled- U gate, which is equivalent to $|1\rangle\langle 1| \otimes U + |0\rangle\langle 0| \otimes I_2$

Right: example of controlled- U gate, when applied to qubits 3 and 4 if qubit 1 is $|0\rangle$ and qubit 2 is $|1\rangle$. In this case controlled- U is equivalent to $|01\rangle\langle 01| \otimes U + (I_4 - |01\rangle\langle 01|) \otimes I_4$.

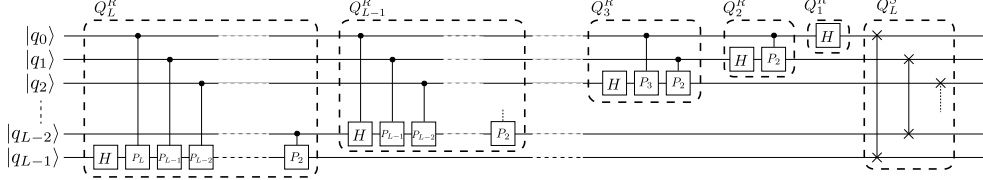
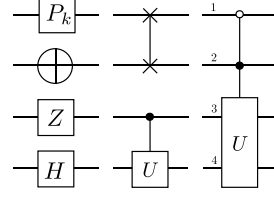


Fig. 2 The circuit of the QFT of L qubits.

work assumes unrestricted access to all single-qubit and two-qubit gates. Consequently, the gate complexity is expressed in terms of the number of single-qubit and two-qubit gates, while disregarding the $O(1/\varepsilon)$ factor associated with the approximation. This paper implicitly assumes that a given quantum circuit and its controlled version, with a constant number of control qubits, exhibit the same asymptotic gate complexity. However, the gate complexity may increase when accounting for the quantum device topology, particularly in scenarios where qubits are not fully connected [37].

Throughout the paper, we use some standard quantum gates given in Eq. (1) with circuit representations described in Figure 1. X , Z and H represent X -Pauli, Z -Pauli, and Hadamard gates, respectively. The SWAP gate swaps the state of two qubits. Phase shift gates P_k map basis states as $P_k|0\rangle = |0\rangle$ and $P_k|1\rangle = e^{2\pi i/2^k}|1\rangle$, where i is the imaginary unit and $|\cdot\rangle$ are vectors in the Dirac notation such that $|0\rangle = (1, 0)^T$ and $|1\rangle = (0, 1)^T$, $\langle \cdot |$ is a conjugate transpose of the vector. U^\dagger is a conjugate transpose of matrix U and \bar{z} is a conjugate of a complex number z . \otimes denotes the tensor product of matrices, and \oplus represents a direct sum of subspaces in one case and a modulo 2 sum in another, with the meaning clear from the context. Finally, $I(\cdot)$ is an indicator function with some condition, for example, $I(x \leq 0) = 1$ if $x \leq 0$, and 0 otherwise, while I_M is an identity matrix of size $M \times M$.

$$\begin{aligned} P_k &= \begin{pmatrix} 1 & 0 \\ 0 & e^{2\pi i/2^k} \end{pmatrix} & X &= \begin{pmatrix} 0 & 1 \\ 1 & 0 \end{pmatrix} & \text{SWAP} &= \begin{pmatrix} 1 & 0 & 0 & 0 \\ 0 & 0 & 1 & 0 \\ 0 & 1 & 0 & 0 \\ 0 & 0 & 0 & 1 \end{pmatrix} \\ Z &= \begin{pmatrix} 1 & 0 \\ 0 & -1 \end{pmatrix} & H &= \frac{1}{\sqrt{2}} \begin{pmatrix} 1 & 1 \\ 1 & -1 \end{pmatrix} \end{aligned} \quad (1)$$

We denote a subroutine of integer comparison on j qubits to some value k as $\text{Comparator}_j(k)$, formally,

$$\text{Comparator}_j(k) |x\rangle |b\rangle \mapsto |x\rangle |b + I(x \geq k) \bmod 2\rangle, \quad (2)$$

which can be implemented by adding two's complement of $-k$ with carry bit representing the result, which in turn requires $O(j)$ gates. We denote a subroutine of cyclic shift of j qubits by some value k as $\text{Adder}_j(k)$, formally,

$$\text{Adder}_j(k) |x\rangle \mapsto |x + k \bmod 2^j\rangle. \quad (3)$$

There are various implementations of this operation [38–40] with various numbers of ancilla qubits required. [38, 39] require $O(j)$ gates and $O(j)$ ancilla qubits. [40] implements the cyclic shift with the use of the quantum Fourier transform (QFT) [41] that requires at most $O(j^2)$ gates and no ancilla qubits.

We extensively use QFT and its subroutines. Recall the transform of size $N = 2^L$,

$$QFT : |x\rangle \mapsto \frac{1}{\sqrt{N}} \sum_{k=0}^{N-1} e^{2\pi i x k / N} |k\rangle,$$

where $|x\rangle$ and $|k\rangle$ are basis states of L qubits. Moreover,

$$|k\rangle = |k_{L-1} \dots k_0\rangle = |k_{L-1}\rangle \otimes |k_{L-2}\rangle \otimes \dots \otimes |k_0\rangle$$

where $k = \sum_{j=0}^{L-1} 2^j k_j$ or $k_{L-1} \dots k_0$ is a binary representation of k . This also implies that we follow the big-endian convention.

The implementation of the QFT of L qubits, Q_L , has a decomposition:

$$Q_L = Q_L^S Q_1^R \dots Q_L^R = Q_L^S \left(\prod_{i=1}^L Q_i^R \right), \quad (4)$$

where Q_i^R is a QFT rotation of i qubits and Q_L^S reverses the order of L qubits. QFT rotation Q_i^R comprises of H -gate applied to qubit $i-1$ followed by phase gates P_{i-j+1} applied to qubit $i-1$ controlled by j for $j = 0, \dots, i-2$. Q_L^S reverses the order by swapping each pair of qubits i and $L-i-1$. Figure 2 depicts a circuit of the QFT of L qubits and highlights its subroutines such as QFT rotations Q_i^R and QFT swap Q_L^S .

The classical counterpart of the QFT is the discrete Fourier transform (DFT) which has a different sign of the exponent. Specifically, the DFT of size N in Dirac's notation is

$$DFT : |x\rangle \mapsto \frac{1}{\sqrt{N}} \sum_{k=0}^{N-1} e^{-2\pi i x k / N} |k\rangle.$$

Therefore, matrix of the DFT of size 2^L is Q_L^\dagger . The DFT, in turn, is a counterpart of the continuous Fourier transform. The Fourier transform of a measurable function $f \in L_2(\mathbb{R})$ is given by the following equation

$$\hat{f}(\xi) = \frac{1}{\sqrt{2\pi}} \int_{-\infty}^{\infty} f(x) e^{-i2\pi x \xi} dx. \quad (5)$$

We refer to f as a function in the spatial domain, and $f(x - x_0)$ is a shift by x_0 in the spatial domain by x_0 . The functions with the circumflex, for example \hat{f} , are considered in the (ordinary) frequency domain, and $\hat{f}(\xi - \xi_0)$ is a shift by ξ_0 in the frequency domain.

When we consider $f : [0, 1] \mapsto \mathbb{R}$ and uniform discretization in the interval $[0, 1]$, $x_k = k/N$ for $k = 0, \dots, N-1$ where $N = 2^L$ for some integer $L \geq 1$. We use brackets to denote the discretization of a function and let $f[k] = f(k/N)$. In the (ordinary) frequency domain, we emphasize that $k \in \mathbb{Z}$ by the square brackets and $\hat{f}[k] = \hat{f}(k)$. Then in the discrete case,

$$(\hat{f}[0], \dots, \hat{f}[N-1])^T = Q_L^\dagger (f[0], \dots, f[N-1])^T.$$

Notice that we use a different range $\{-N/2, \dots, N/2 - 1\}$ in the discretization of \hat{f} , however, $\hat{f}[-N/2 + k] = \hat{f}[N/2 + k]$.

2.2 Wave packets

In the paper, we design algorithms that implement wave packet transforms for wave packets with compact frequency support. Moreover, we define wave packets exclusively in the frequency domain, although the wave packets in the spatial domain can be obtained via inverse Fourier transform. We index wave packets $\varphi_{m,n}^j$ by three indices: their scale $j \in \mathbb{Z}_+ \setminus \{0\}$, frequency $m \in \mathbb{Z}_+$, and position in space $n \in \mathbb{Z}$. Here, \mathbb{Z}_+ denotes nonnegative integer numbers.

First, we consider wave packets with sharp frequency windows such that generating functions are based on perfect filters:

$$\begin{aligned} \hat{\varphi}_m^0(\xi) &= I \{2\xi \in [-m-1, -m) \cup [m, m+1)\}, \\ \hat{\varphi}_m^j(\xi) &= 2^{-j/2} \hat{\varphi}_m^0(2^{-j}\xi), \\ \hat{\varphi}_{m,n}^j(\xi) &= e^{-i2\pi n 2^{-j} \cdot \xi} \hat{\varphi}_m^j(\xi). \end{aligned} \tag{6}$$

The support of $\hat{\varphi}_{m,n}^j$ is centered in frequency around $\pm\xi_{j,m} = \pm 2^{j-1}m$ and in space around $x_{j,n} = 2^{-j}n$. The resulting wave packets are *Shannon wavelets*. The classical indexation arising from multipass filters differs from the above and requires a simple permutation (see Chapter 8 of [4] for details).

The *1D wave atoms* introduced in [9] are based on non-standard wavelets of [11], and are similarly centered in frequency around $\pm\xi_{j,m} = \pm 2^{j-1}m$ and centered in space around $x_{j,n} = 2^{-j}n$:

$$\begin{aligned} \hat{\psi}_m^j(\xi) &= 2^{-j/2} \hat{\psi}_m^0(2^{-j}\xi), \\ \hat{\psi}_{m,n}^j(\xi) &= e^{-i2\pi n 2^{-j} \cdot \xi} \hat{\psi}_m^j(\xi). \end{aligned} \tag{7}$$

Its mother wave packets demonstrate an elegant way to deal with the problem of frequency localization [9, 11] and involve symmetric pairs of compactly supported bumps in the frequency domain:

$$\hat{\psi}_m^0(\xi) = e^{-i\pi\xi} [e^{i\alpha_m} g((-1)^m(2\pi\xi - 2\alpha_m)) + e^{-i\alpha_m} g((-1)^{m+1}(2\pi\xi + 2\alpha_m))], \tag{8}$$

where $\alpha_m = \frac{\pi}{2}(m + \frac{1}{2})$ and g is a continuous real-valued function compactly supported on an open interval $(-\frac{7}{6}\pi, \frac{5}{6}\pi)$. Furthermore, g must satisfy the following requirements: for any $w \in [-\frac{\pi}{3}, \frac{\pi}{3}]$,

$$g^2(\frac{\pi}{2} - w) + g^2(\frac{\pi}{2} + w) = 1, \quad (9)$$

$$g(-2w - \frac{\pi}{2}) = g(\frac{\pi}{2} + w). \quad (10)$$

The above construction can be understood qualitatively in the following way. First, one can write the support of g as the union of two intervals:

$$A_1 = [-\frac{7}{6}\pi, \frac{1}{6}\pi], \quad A_2 = [\frac{1}{6}\pi, \frac{5}{6}\pi]. \quad (11)$$

Typically g is chosen to be monotonically increasing on A_1 , and monotonically decreasing on A_2 . In Eq. (9), $g(\frac{\pi}{2} - w)$ and $g(\frac{\pi}{2} + w)$ can be understood as mirror images of each other, reflected around the midpoint of the interval A_2 . In the wave atom transform, these mirror images are associated with neighboring wavepackets, and Eq. (9) says that their squares sum to 1. Eq. (10) says that the increasing part of g (on the interval A_1 , centered at $-\pi/2$) is a mirror image of the decreasing part of g (on the interval A_2 , centered at $\pi/2$), stretched by a factor of 2. This asymmetric property (10) of profile g is important to preserve the orthogonality of the $\hat{\psi}_{m,n}^j$. In contrast to Shannon wavelets, wave atoms have overlapping support in the frequency domain.

One can describe the wavepackets $\hat{\psi}_m^0(\xi)$ qualitatively as follows. In Eq. (8), $\hat{\psi}_m^0(\xi)$ consists of a complex phase factor of $e^{-i\pi\xi}$, times a linear combination of two bumps, which are supported near $\pm\alpha_m/\pi = \pm\frac{1}{2}(m + \frac{1}{2})$. These two bumps are mirror images of each other, with a relative phase difference of $e^{2i\alpha_m} = \mathbf{i}(-1)^m$. Furthermore, when comparing wavepackets $\hat{\psi}_m^0(\xi)$ and $\hat{\psi}_{m+1}^0(\xi)$ that are adjacent to each other in the frequency domain, one sees that the bumps corresponding to m overlap with, and are mirror images of, the bumps corresponding to $m + 1$. In other words, the shapes of the wavepackets $\hat{\psi}_m^0(\xi)$ change according to the parity of m .

Because of the above properties, these wavepackets form an orthonormal basis so that for the square-integrable function $f \in L^2(\mathbb{R})$,

$$f = \sum_{j,m} \sum_n \langle f, \psi_{m,n}^j \rangle \psi_{m,n}^j = \sum_{j,m} \sum_n c_{j,m,n} \psi_{m,n}^j. \quad (12)$$

For all (j, m) , the coefficients $c_{j,m,n}$ can be interpreted as a convolution at scale 2^{-j} and are defined by Plancherel's theorem as follows:

$$\begin{aligned} c_{j,m,n} &= \langle f, \psi_{m,n}^j \rangle = \int \psi_{m,n}^j(x) f(x) dx \\ &= \int \psi_m^j(x - 2^{-j}n) f(x) dx = \frac{1}{2\pi} \int e^{i2\pi 2^{-j}n\xi} \overline{\hat{\psi}_m^j(\xi)} \hat{f}(\xi) d\xi. \end{aligned} \quad (13)$$

We consider $f : [0, 1] \mapsto \mathbb{R}$ and its uniform discretization on the interval, $f[k] = f(k/N)$ for $k = 0, \dots, N-1$ where $N = 2^L$ for some integer $L \geq 1$. Then, up to some

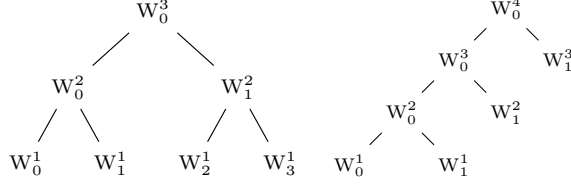


Fig. 3 Examples of trees that generate wavelet packet bases. Left: a perfect binary tree, which generates a uniform wavelet packet basis. Right: a dyadic tree, which generates a dyadic wavelet packet basis.

small error, the discrete version of the transform is

$$c_{j,m,n} \approx c_{j,m,n}^D = \sum_{k=-N/2, \dots, N/2-1} \overline{\hat{\psi}_{m,n}^j(k)} \hat{f}[k]. \quad (14)$$

Therefore, the operation of our interest is

$$f[0], \dots, f[N-1] \mapsto \{c_{j,m,n}^D\}_{(j,m,n) \in \Gamma}, \quad (15)$$

where $\{\hat{\psi}_{m,n}^j\}_{(j,m,n) \in \Gamma}$ organize an orthogonal basis for some set of index triplets Γ . We discuss the selection of orthogonal bases in the next section.

2.3 Wavelet packet trees

Coifman, Meyer, and Wickerhauser introduced wavelet packets by linking multiresolution approximations (a sequence of embedded vector spaces $(V_j)_{j \in \mathbb{Z}}$ for approximating $L_2(\mathbb{R})$ functions) with wavelets [42]. They decompose a multiresolution approximation space V_j into a lower-resolution space V_{j+1} and a detail space W_{j+1} by splitting the orthogonal basis into two new orthogonal bases. Intuitively, when wavelets are used for image processing, we may lose some details when reducing the resolution. [42] also show that, instead of just dividing the approximation spaces to create the so-called detail spaces and wavelet bases, we can split the detail spaces to generate new bases. This process of dividing vector spaces can be represented in a structure of a binary tree (see Chapter 8 of [4]). Any node in this binary tree can be labeled by (j, m) , where j is the level of the tree, and m is the number of nodes on its left at the same level. To each node we associate a space W_m^j , which admits an orthogonal basis $\{\varphi_{m,n}^j\}_{n \in \mathbb{Z}}$.

We adopt the notion of wavelet packet trees and associate W_m^j with an orthogonal basis $\{\hat{\psi}_{m,n}^j\}_{n \in \mathbb{Z}}$ which in the discrete case becomes $\{\hat{\psi}_{m,n}^j\}_{0 \leq n < 2^j}$ for wave atoms or $\{\hat{\varphi}_{m,n}^j\}_{0 \leq n < 2^j}$ for the Shannon wavelet. Then, all W_m^j can be organized into a binary wavelet packet tree. We will abuse the notation and refer to W_m^j as both the space spanned by the basis $\{\hat{\psi}_{m,n}^j\}_{0 \leq n < 2^j}$ (or $\{\hat{\varphi}_{m,n}^j\}_{0 \leq n < 2^j}$) and the node in the tree.

Definition 1 (Admissible wavelet packet binary tree, adapted [4]). *A binary tree of height $L-1$ with nodes $\{W_m^j\}$ is admissible if*

1. The root of the tree is W_0^L ,

2. Every non-leaf node W_m^j has two children W_{2m}^{j-1} and W_{2m+1}^{j-1} , and $j \geq 2$.

Using definition 1, one can construct wavelet bases $\{\varphi_{m,n}^j \mid (j, m, n) \in \Gamma_T\}$, where Γ_T is the set of index triplets generated by the wave packet admissible tree T :

$$\Gamma_T = \{(j, m, n) \mid W_m^j \in \Lambda_T \text{ and } 0 \leq n < 2^j\}, \quad (16)$$

$$\Lambda_T = \{W_m^j \mid W_m^j \text{ is a leaf-node in } T\}. \quad (17)$$

The two of more popular bases generated by wavelet packet trees [4] are the following:

- *Uniform* $\{\varphi_{m,n}^j\}$, where j 's are equal to some fixed value (call it j_0), and $\Gamma = \{(j, m, n) \mid 0 \leq m < 2^{L-j}, 0 \leq n < 2^j, j = j_0\}$. This type of basis is generated by perfect binary trees.
- *Dyadic* $\{\varphi_{m,n}^j\}$. In this case, most of the basis function has $m = 1$, and $\Gamma = \{(1, 0, 0), (1, 0, 1)\} \cup \{(j, 1, n) \mid 1 \leq j < L, 0 \leq n < 2^j\}$. This type of basis is generated by dyadic trees (such that every right node is a leaf while every left node is nonleaf unless the node is on the minimal level).

The examples of wavelet packet trees generating orthogonal bases discussed above can be found in Figure 3. One can verify that both approaches render an orthogonal basis for Shannon wavelets and wave atoms. In sections 3.2 and 5.2, we will construct another class of trees that generate orthogonal bases for the wave atom transform, and have an additional property: “parabolic scaling,” $m = O(2^j)$, which is desirable for many applications of the wave atom transform [9].

We would also like to state a few properties of admissible wave packet trees that will be helpful in the later discussion.

Proposition 1 (enumeration properties of admissible wave packet tree). *For wave packet admissible tree T (by definition 1) with a root W_0^L and K leaf nodes $\{W_{m_i}^{j_i} \mid i = 1, \dots, K\}$ traversed from left to right,*

1. $m_1 = 0$,
2. For $i = 1, \dots, K - 1$, $(m_i + 1)2^{j_i} = m_{i+1}2^{j_{i+1}}$,
3. $(m_K + 1)2^{j_K} = 2^L$.

Proof. See Appendix B.1. □

3 Encoding

The transform of interest in equation (15) does not define an order of the coefficients $c_{j,m,n}^D$. In other words, $\hat{\varphi}_{m,n}^j$ and $\hat{\psi}_{m,n}^j$ need to be indexed. Moreover, in equation (14) the sum goes over negative and positive integer frequencies. We would like to encode both the wave packet indices (j, m, n) and the (integer) frequencies k such that each is represented by L bits.

3.1 Frequency encoding

This section introduces frequency encoding and decoding procedures, where encoded frequencies are represented by L bits. It also covers the concept of retaining decoding, allowing a subset of bits to be decoded without affecting others, and involves constructing corresponding quantum circuits.

Given that both Shannon wavelets and wave atoms are symmetric around zero, we would like to map the frequencies of the same absolute value with different sign in such a way that they would have consecutive indices when encoded. Moreover, it is natural to expect that the nonnegative frequency k would have a smaller encoded index than the frequency $k + 1$.

In order to accomplish this, we introduce a *frequency encoding procedure* as a bijection $e : \{-N/2, \dots, N/2 - 1\} \rightarrow \{0, \dots, N - 1\}$ given by

$$e(k) = \begin{cases} 2k, & k \geq 0, \\ 2|k| - 1, & k < 0. \end{cases} \quad (18)$$

We call the reverse procedure of (18) *frequency decoding procedure* and define it by the inverse mapping $d : \{0, \dots, N - 1\} \rightarrow \{-N/2, \dots, N/2 - 1\}$ given by

$$d(i) = \begin{cases} \frac{1}{2}i, & i \text{ even}, \\ -\frac{1}{2}(i + 1), & i \text{ odd}. \end{cases} \quad (19)$$

We also introduce a *retaining decoding procedure* $\tilde{d}(\cdot, j, m) : \{0, \dots, 2^j - 1\} \rightarrow \{0, \dots, 2^j - 1\}$ such that for $c \in \{0, \dots, 2^j - 1\}$

$$\tilde{d}(c, j, m) = d(m2^j + c) \bmod 2^j. \quad (20)$$

The word “retaining” refers to the idea of staying in range of size 2^j (which will be fully explored in section 4) and the argument c corresponds to the indices within the range of desired size. We can compute \tilde{d} as follows

$$\tilde{d}(c, j, m) = \begin{cases} 2^{j-1}I(m \text{ is odd}) + \frac{1}{2}c, & \text{if } c \text{ is even,} \\ 2^j - 2^{j-1}I(m \text{ is odd}) - \frac{1}{2}(c + 1), & \text{if } c \text{ is odd.} \end{cases} \quad (21)$$

3.1.1 Frequency encoding circuit

Both Shannon wavelet and wave atom transforms include DFT (inverse QFT) as the initial step to transform the spatial domain into the frequency domain. However, the result of DFT is defined on a grid $\{0, \dots, N - 1\}$, but our transforms are defined on a grid $\{-N/2, \dots, N/2 - 1\}$. Due to the periodicity of Fourier transform $\hat{f}[k] = \hat{f}[k - N]$,

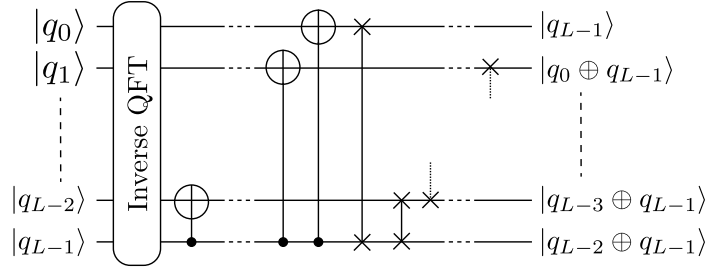


Fig. 4 Frequency encoding circuit which implements function $e(\cdot)$ coupled with Q_L^\dagger .

we have the initial stage as follows

$$Q_L^\dagger \left(\sum_{k=0}^{N-1} f[k] |k\rangle \right) = \sum_{k=0}^{N-1} \hat{f}[k] |k\rangle = \sum_{k=0}^{N/2-1} \hat{f}[k] |k\rangle + \sum_{k=-N/2}^{-1} \hat{f}[k] |k+N\rangle.$$

We transform $|k\rangle$ into $|e(k)\rangle$ when $k \geq 0$ and $|k+N\rangle$ into $|e(k)\rangle$ when $k < 0$ as described in (18). The further steps of the transforms are based on

$$\sum_{k=-N/2}^{N/2-1} \hat{f}[k] |e(k)\rangle = \sum_{k=0}^{N-1} \hat{f}[d(k)] |k\rangle.$$

The two initial steps of the transforms, the inverse QFT and frequency encoding, are expressed in Algorithm 1 with its circuit shown in Figure 4. The gate complexity of the algorithm is $O(L^2)$ due to the QFT step.

3.1.2 Retaining decoding circuit

Recall the retaining decoding procedure defined by (20). Notice that $\tilde{d}(c, j, m) = \tilde{d}(c, j, m \bmod 2)$ meaning that the retaining decoding procedure depends on the parity of m rather than the value. Considering the parity of m we may construct the quantum circuit of $\tilde{d}(\cdot, j, m)$ that operates on $j+1$ qubits: j qubits in representation of c and 1 qubit of m_0 where m_0 is the least significant qubit of m . We refer to this circuit as \tilde{D}_j . The implementation of \tilde{D}_j is provided in Algorithm 2 with gate complexity of $O(j)$, its correctness is shown in the Appendix B.2.

In the special case of $j = L$, we do not pass the parity of m to the algorithm and assume that $m_0 = 0$.

Algorithm 1 QFT and frequency encoding

Input: $\sum_{q=0}^{2^L-1} f[q] |q\rangle$.

Result: $\sum_{q=0}^{2^L-1} \hat{f}[d(q)] |q\rangle$.

1. Apply Q_L^\dagger (equivalent to DFT). This produces the state:

$$\sum_{q=0}^{2^L-1} \hat{f}[q] |q_{L-1}\rangle |q_{L-2}\rangle \dots |q_0\rangle$$

2. For each $i = 0, \dots, L-2$, apply controlled- X gate to qubit i controlled on qubit $L-1$. This produces the state:

$$\sum_{q=0}^{2^L-1} \hat{f}[q] |q_{L-1}\rangle |q_{L-2} \oplus q_{L-1}\rangle \dots |q_0 \oplus q_{L-1}\rangle.$$

3. Cyclic shift of L qubits implemented by SWAP gates. This produces the state:

$$\sum_{q=0}^{2^L-1} \hat{f}[q] |q_{L-2} \oplus q_{L-1}\rangle \dots |q_0 \oplus q_{L-1}\rangle |q_{L-1}\rangle$$

3.2 Wave packet encoding

The wavelet packet transform (15) can be written as

$$\sum_{k=0}^{N-1} f[k] |k\rangle \mapsto \sum_{(j,m,n) \in \Gamma_T} c_{j,m,n}^D |(j,m,n)\rangle,$$

where $N = 2^L$, each $c_{j,m,n}^D \approx \langle f, \psi_{m,n}^j \rangle$ and $|(j,m,n)\rangle$ is a representation of the triplet (j,m,n) . In this section, we discuss the encoding of such triplets using L bits. To do this, we will introduce data structures for representing wave packet trees.

Consider an admissible wave packet tree T (in the sense of Definition 1), described by the set of its leaf nodes $\Lambda_T = \{W_m^j\}$. By Proposition 1, the mapping

$$(j,m,n) \mapsto p = m2^j + n \tag{22}$$

is a bijection between the set of index triplets $\Gamma_T = \{(j,m,n) \mid W_m^j \in \Lambda_T, 0 \leq n < 2^j\}$ and the range of $\{0, \dots, N-1\}$. Observe that j least significant bits of the encoded index p represent n in binary form, while the remaining bits represent m . Therefore, to decode the index, we need to know j . This requires information about the structure of the tree T .

Algorithm 2 Retaining decoding circuit \tilde{D}_j

Input: $|m_0\rangle \sum_{q=0}^{2^j-1} \alpha_q |q\rangle$ where $m_0 \in \{0, 1\}$.

Result: $|m_0\rangle \sum_{q=0}^{2^j-1} \alpha_q |\tilde{d}(q, j, m_0)\rangle$.

1. For each qubit $i = 1, \dots, j-1$, apply X gate to qubit i controlled on qubit 0. This produces the state:

$$|m_0\rangle \sum_{q=0}^{2^j-1} \alpha_q |q_{j-1} \oplus q_0\rangle \dots |q_1 \oplus q_0\rangle |q_0\rangle.$$

2. Cyclic shift of j qubits implemented by SWAP gates. This produces the state:

$$|m_0\rangle \sum_{q=0}^{2^j-1} \alpha_q |q_0\rangle |q_{j-1} \oplus q_0\rangle \dots |q_1 \oplus q_0\rangle.$$

3. Apply X gate to qubit $j-1$ controlled on qubit j . This produces the state:

$$|m_0\rangle \sum_{q=0}^{2^j-1} \alpha_q |q_0 \oplus m_0\rangle |q_{j-1} \oplus q_0\rangle \dots |q_1 \oplus q_0\rangle.$$

3.2.1 Encodings of wave packet trees

We will construct algorithms for implementing wave packet transforms, given access to information about the wave packet tree T through the following mechanism. Let us define a function $\tilde{h} : \{0, \dots, N-1\} \mapsto \{1, \dots, L-1\}$ such that

$$\forall (j, m, n) \in \Gamma_T, \quad \tilde{h}(m2^j + n) = j. \quad (23)$$

In other words, the function \tilde{h} maps the encoded index p back to j .

Furthermore, we define a family of *helper decoding boolean functions* $h_j : \{0, \dots, N-1\} \mapsto \{0, 1\}$ for $1 \leq j < L$ such that

$$h_j(p) = 1 \text{ if and only if } \tilde{h}(p) \geq j. \quad (24)$$

Note that the function $\tilde{h}(\cdot)$ and the family of functions $h_j(\cdot)$ allows us to decode p 's.

In this paper, we assume that there is an efficient implementation of functions h_j , specifically

$$|p\rangle |b_1 \dots b_{L-1}\rangle \mapsto |p\rangle |b_1 \oplus h_1(p), \dots, b_{L-1} \oplus h_{L-1}(p)\rangle$$

can be implemented using $O(L^2)$ gates. We demonstrate that this is possible for specific kinds of wave packet trees:

- *Tree generating uniform basis.* All j 's of leaf nodes in the wave packet tree are equal, say $j = j'$, so $h_j(p) = I(j \geq j')$, with the implementation using one X -gate.
- *Dyadic tree.* Observe that $h_{L-1}(p) = p_{L-1}$, $h_{L-2}(p) = h_{L-1}(p) \vee p_{L-2} = p_{L-1} \vee p_{L-2}$, in general,

$$h_i(p) = \vee_{i'=i}^{L-1} p_{i'} = h_{i+1}(p) \vee p_i \text{ for } i = 2, \dots, L-2,$$

and $h_1(p) = 1$, where \vee is a logical OR operator. The procedure requires $O(L)$ gates.

- *Monotonic tree.* We say that the wave packet tree T is monotonically increasing if $j_{i+1} \geq j_i$ for all i when the tree's leaf nodes are ordered from left to right. Denote by m_j^* , index m of the leftmost leaf node on the level j . If no leaf nodes are on the level, m_j^* is the index of the node which could be next to the most right node on level j , that is, $m_j^* - 1$ is the index of the most right node. If there are no nodes on the level, let $m_j^* = 0$. Then

$$h_j(p) = I(p \geq m_j^* 2^j).$$

Given p is L -bit value, the comparison requires $O(L)$ classical bit operations or quantum gates. The total number of gates for the procedure to compute all $h_j(p)$, $1 \leq j < L$, is $O(L^2)$.

Recall that the wave atom transform requires that for any W_m^j , $m = O(2^j)$, which constitutes a parabolic tree and is covered by the case of monotonic trees. In the paper, we focus on monotonic trees and assume that all trees of interest are encoded by the indices of the leftmost leaf nodes at each level, m_j^* 's. This tree representation requires $O(L^2)$ bits and, therefore, does not increase the complexity of circuit construction.

4 Quantum Shannon wavelet transform

In this section, we demonstrate how the retaining decoding function \tilde{d} and the helper decoding functions h_j can be used to construct an efficient implementation of the quantum Shannon wavelet transform for a monotonic tree (see Theorem 2).

Recall the definition of Shannon wavelets $\hat{\varphi}_m^j$ by equation (6),

$$\hat{\varphi}_m^j(\xi) = 2^{-j/2} I \{ 2^{-j+1} \xi \in [-m-1, -m) \cup [m, m+1) \}.$$

See figure 5 for a visualization of Shannon wavelet. It is straightforward to see that for any wave packet admissible tree T generating a transform of size $N = 2^L$, each frequency $k \in [-N/2, N/2)$ is in the support of one Shannon wavelet $\hat{\varphi}_m^j$ corresponding to a leaf node $W_m^j \in \Lambda_T$. With the inclusion of shifts in the spatial domain,

$$\hat{\varphi}_{m,n}^j(\xi) = e^{-i2\pi n 2^{-j} \cdot \xi} \hat{\varphi}_m^j(\xi), \quad (25)$$

and following the definition of the discrete wave packets transform (14), we can formally define the quantum Shannon wavelet transform.

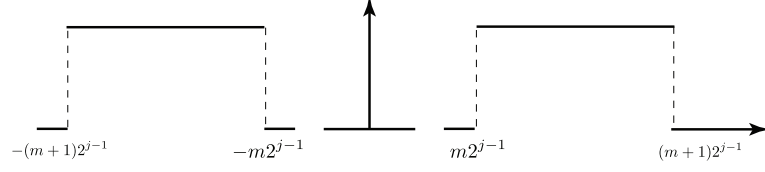


Fig. 5 Shannon wavelet $\hat{\varphi}_m^j$: one bump per each side of the axis in the frequency domain.

Definition 2. Consider an admissible wave packet tree T with a root node W_0^L . Define a matrix C^S as

$$C_{m2^j+n,i}^S = \overline{\hat{\varphi}_{m,n}^j(d(i))}, \quad (26)$$

where $W_m^j \in \Lambda_T$, d is the decoding function in equation (19), and $n, i \in \mathbb{Z}$ such that $0 \leq n < 2^j$ and $0 \leq i < N$. The following transform of size $N = 2^L$, where Q_L is QFT,

$$\sum_{k=0}^{N-1} f[k] |k\rangle \mapsto \sum_{W_m^j \in \Lambda_T} \sum_{n=0}^{2^j-1} \left(\sum_{i=0}^{N-1} C_{m2^j+n,i}^S \hat{f}[d(i)] \right) |m2^j + n\rangle \quad (27)$$

$$\text{where } \hat{f}[k] = \begin{cases} \sum_{i=0}^{N-1} (Q_L^\dagger)_{ki} f[i], & \text{if } k \geq 0, \\ \sum_{i=0}^{N-1} (Q_L^\dagger)_{(k+N)i} f[i], & \text{if } k < 0, \end{cases}$$

is called a quantum Shannon wavelet transform.

The Shannon wavelet transform has a block structure, which allows it to be implemented efficiently by a quantum circuit, as follows. When we consider a leaf node $W_m^j \in \Lambda_T$ and $n = 0, \dots, 2^j - 1$, $C_{m2^j+n,i}^S$ can be expressed as follows

$$\begin{aligned} C_{m2^j+n,i}^S &= \overline{\hat{\varphi}_{m,n}^j(d(i))} \\ &= 2^{-j/2} e^{i2\pi 2^{-j} n \cdot d(i)} I \{d(i) \in [-(m+1)2^{j-1}, -m2^{j-1}] \cup [m2^{j-1}, (m+1)2^{j-1}]\} \\ &= 2^{-j/2} e^{i2\pi 2^{-j} n \cdot d(i)} I \{i \in [m2^j, (m+1)2^j]\}. \end{aligned}$$

Denote $c = i - m2^j$, then

$$C_{m2^j+n,m2^j+c}^S = 2^{-j/2} e^{i2\pi 2^{-j} n \cdot d(m2^j+c)} I \{0 \leq c < 2^j\}.$$

This implies that C^S is a block diagonal matrix with blocks of size $2^j \times 2^j$ for each leaf node $W_m^j \in \Lambda_T$. Let us denote the block corresponding to W_m^j by $F^S(j, m)$. See Figure 6 for an example of the block-diagonal structure of C^S . Furthermore, given the periodicity of the exponent term of $C_{m2^j+n,m2^j+c}^S$, we can replace $d(m2^j + c)$ with $\tilde{d}(j, m, c)$ by definition (20). Then for $W_m^j \in \Lambda_T$, $0 \leq n, c < 2^j$,

$$C_{m2^j+n,m2^j+c}^S = (F^S(j, m))_{n,c} = 2^{-j/2} e^{i2^{-j} 2\pi n \cdot \tilde{d}(c,j,m)}. \quad (28)$$

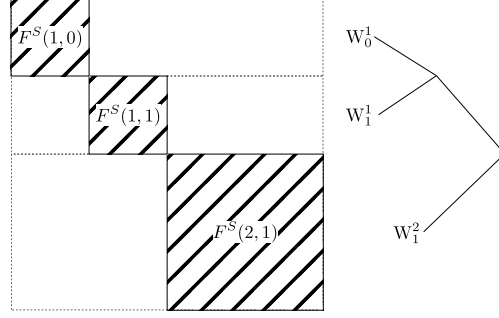


Fig. 6 Block-diagonal structure of matrix C^S with the blocks $F^S(1,0)$, $F^S(1,1)$ and $F^S(2,1)$ corresponding to leaf nodes of $T = \{W_0^1, W_1^1, W_1^2\}$.

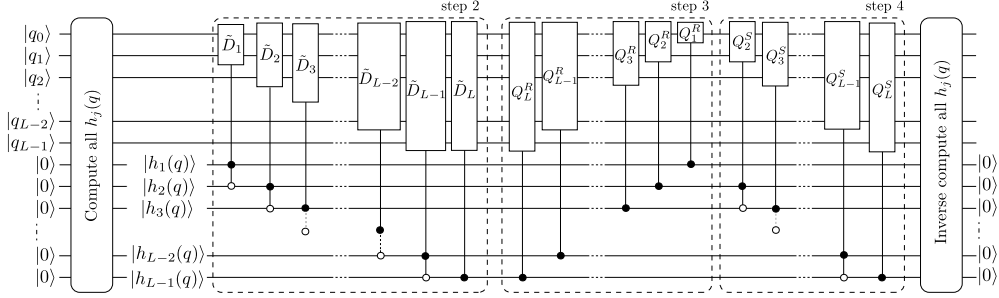


Fig. 7 Quantum circuit implementing Shannon wavelet transform C^S of size 2^L . The family of boolean functions h_j is defined in (24), the retaining decoding circuits \tilde{D}_j are presented in Algorithm 2. Q_j^R and Q_j^S are steps of Fourier transform, see (4).

This can also be written more compactly as:

$$C^S = \bigoplus_{W_m^j \in \Lambda_T} F^S(j, m). \quad (29)$$

In this way $F^S(j, m)$ consists of two actions: (1) decoding \tilde{d} , and (2) QFT on j qubits. For the decoding \tilde{d} we pass $j + 1$ qubits to the retaining decoding circuit \tilde{D}_j (Algorithm 2), where the most significant qubit gives parity of m . To know j we use the helper decoding functions h_j by definition (24). Finally, we apply QFT on j qubits controlled by the state of ancilla qubits in the state of value of h_j 's. We combine these steps in Algorithm 4 (see Appendix A.1), with the corresponding quantum circuit in Figure 7. The total gate complexity of the algorithm is $O(L^2)$.

Theorem 2. *Let T be a monotonic wave packet admissible tree defined for discretization of size $O(2^L)$. If T is represented by the leftmost node on each level, then the gate complexity of quantum Shannon wavelet transform generated by the tree T is $O(L^2)$. The complexity of the circuit construction is $O(L^2)$.*

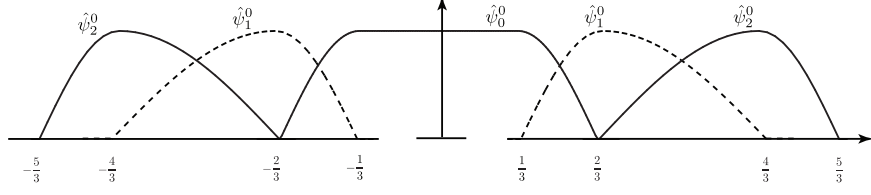


Fig. 8 Wave atoms. $\hat{\psi}_0^0$ is unique, $\hat{\psi}_1^0$ is an example of odd m 's, $\hat{\psi}_2^0$ represents even m 's.

Proof See Appendix A.1. □

5 Quantum wave atom transform

In this section, we define and implement the quantum wave atom transform in one dimension, and we prove that it is efficient, for a variety of choices of the mother wave atom and the wave atom tree structure (see Theorem 7 and Corollary 8). This is a step towards implementing two-dimensional wave atoms, which have numerous applications [9], on a quantum computer.

To do this, we address two technical issues. First, in contrast to the Shannon wavelet transform, wave atoms have supports that overlap in the frequency domain; therefore, the wave atom transform requires considering the “blending” of the elements of \hat{f} .

Second, for many applications, it is desirable to use wave atoms that obey a “parabolic” scaling relationship, i.e., wavelength \sim (diameter of support)² [9]. In order to do this, it is necessary to use more general classes of wave packet trees (introduced in Section 3.2), combined with a specific construction of wave packets that allows neighboring wave packets to have different scales (due to Villemoes [11], and described in Section 2.2).

These techniques are quite flexible, and can be used to implement quantum wave atom transforms based on a variety of wave packet tree structures (see Theorem 7), including monotonic trees (see Corollary 8).

5.1 Wave atoms’ support over the frequency domain

Recall the definition of wave atoms $\hat{\psi}_m^j$ by equations (7) and (8),

$$\hat{\psi}_m^j(\xi) = 2^{-j/2} \hat{\psi}_m^0(2^{-j}\xi),$$

$$\hat{\psi}_m^0(\xi) = e^{-i\pi\xi} [e^{i\alpha_m} g((-1)^m(2\pi\xi - 2\alpha_m)) + e^{-i\alpha_m} g((-1)^{m+1}(2\pi\xi + 2\alpha_m))],$$

where $\alpha_m = \frac{\pi}{2}(m + \frac{1}{2})$. The structure of wave atom is dictated by the function g and its properties. Given that the support of function g is $(-\frac{7}{6}\pi, \frac{5}{6}\pi)$, we derive the support of the wave atom $\hat{\psi}_m^j$ over the frequency domain:

$$\begin{aligned} 2^{j-1}(-\frac{4}{3}, \frac{2}{3}) \cup 2^{j-1}(-\frac{2}{3}, \frac{4}{3}) &= 2^{j-1}(-\frac{4}{3}, \frac{4}{3}), \text{ if } m = 0, \\ 2^{j-1}(-(m + \frac{5}{3}), -(m - \frac{1}{3})) \cup 2^{j-1}((m - \frac{1}{3}), (m + \frac{5}{3})) &, \text{ if } m \text{ is odd,} \\ 2^{j-1}(-(m + \frac{4}{3}), -(m - \frac{2}{3})) \cup 2^{j-1}((m - \frac{2}{3}), (m + \frac{4}{3})) &, \text{ if } m \text{ is even.} \end{aligned} \quad (30)$$

(See Figure 8.) The support of each wave atom consists of two intervals, one for negative and one for positive frequencies. This can be rewritten as a union of four intervals with centers $\pm 2^{j-1}m$ and $\pm 2^{j-1}(m+1)$, as follows:

$$\begin{aligned} & \pm 2^{j-1} \left(-\frac{2}{3}, \frac{2}{3}\right) \cup \pm 2^{j-1} \left(1 - \frac{1}{3}, 1 + \frac{1}{3}\right), \text{ if } m = 0, \\ & \pm 2^{j-1} \left(m - \frac{1}{3}, m + \frac{1}{3}\right) \cup \pm 2^{j-1} \left((m+1) - \frac{2}{3}, (m+1) + \frac{2}{3}\right), \text{ if } m \text{ is odd,} \\ & \pm 2^{j-1} \left(m - \frac{2}{3}, m + \frac{2}{3}\right) \cup \pm 2^{j-1} \left((m+1) - \frac{1}{3}, (m+1) + \frac{1}{3}\right), \text{ if } m \text{ is even.} \end{aligned} \quad (31)$$

Let's denote those intervals centered around $\pm 2^{j-1}m$ and $\pm 2^{j-1}(m+1)$ as $\chi_{\pm 2^{j-1}m}$ and $\chi_{\pm 2^{j-1}(m+1)}$ correspondingly. That is why (30) can be rewritten in general case as

$$\chi_{-2^{j-1}(m+1)} \cup \chi_{-2^{j-1}m} \cup \chi_{2^{j-1}m} \cup \chi_{2^{j-1}(m+1)} \quad (32)$$

We will implement a discrete wave atom transform, by restricting to integer frequencies only. For this purpose, let us denote the integer part of the half interval lengths of $\chi_{\pm 2^{j-1}m}$ and $\chi_{\pm 2^{j-1}(m+1)}$ by $\mu_0(j, m)$ and $\mu_1(j, m)$ respectively. Observe that they are equal to

$$\mu_0(j, m) = \lfloor 2^{j-I(m \text{ is odd})}/3 \rfloor, \quad \mu_1(j, m) = \lfloor 2^{j-I(m \text{ is even})}/3 \rfloor. \quad (33)$$

Proposition 3 (Integer support of wave atoms). *An integer frequency $k \in \mathbb{Z}$ is in the support of $\hat{\psi}_m^j$ if and only if*

$$||k| - 2^{j-1}m| \leq \mu_0(j, m) \text{ or } ||k| - 2^{j-1}(m+1)| \leq \mu_1(j, m).$$

Proof. See Appendix B.3. □

One can notice that the intersection of the intervals consists of one point $\chi_{2^{j-1}(m+1)} \cap \chi_{2^{j-1}m} = \{2^{j-1}m + 2^{j-I(m \text{ is odd})}/3\}$ and this value is always fractional, so there is no $k \in \mathbb{Z}$ such that

$$||k| - 2^{j-1}m| \leq \mu_0(j, m) \text{ and } ||k| - 2^{j-1}(m+1)| \leq \mu_1(j, m).$$

5.2 Wave atom admissible trees

We would like to construct a (discrete) wave atom transform based on an admissible wave packet tree T . Here, we state some conditions on T that are sufficient to ensure that the resulting wave atom basis is orthogonal.

We would like every integer $k \in \{-N/2, \dots, N/2 - 1\}$ to lie in the support of two wave atoms, unless k is close to zero (which is covered by a single wave atom) or close to $\pm N$ (which is treated as a special case). As such when we consider two neighboring leaf nodes $W_m^j, W_{m'}^{j'} \in \Lambda_T$, where W_m^j is the left neighbor, we require that the intervals centered around $\pm(m+1)2^j$ related to the two nodes are of equal length,

$$\mu_1(j, m) = \mu_0(j', m'). \quad (34)$$

We define the subset of all wave packet admissible trees that satisfy the condition in equation (34).

Definition 3. Consider an admissible wave packet tree with a root W_0^L and K leaf nodes $\{W_{m_i}^{j_i} \mid i = 1, \dots, K\}$ traversed from left to right. If the following conditions hold for all $i \in \{1, \dots, K-1\}$:

1. $|j_i - j_{i+1}| \leq 1$,
2. if $j_{i+1} = j_i + 1$, then both m_i and m_{i+1} are odd,
3. if $j_{i+1} = j_i - 1$, then both m_i and m_{i+1} are even,

we call such a tree a wave atom admissible tree.

It is straightforward to see that other admissible wave packet trees do not satisfy the condition (34) for some pair of neighboring leaf nodes of the tree. Given the Definition 3 and its reliance on the condition (34), we state an evident property of the wave atom admissible trees.

Proposition 4. Consider a wave atom admissible tree T with a root node W_0^L . Denote by $W_0^{j_l}$ and $W_{m_r}^{j_r}$ the leftmost and rightmost leaf nodes respectively. For any $k \in \{-N/2, \dots, N/2 - 1\}$, where $N = 2^L$, the following holds:

1. If $|k| \leq \mu_0(j_l, 0)$, then k is in the support of only $\hat{\psi}_0^{j_l}$;
2. If $|k| > m_r 2^{j_r-1} + \mu_0(j_r, m_r)$, then k is in the support of only $\hat{\psi}_{m_r}^{j_r}$;
3. Otherwise, k is in the support of exactly two wave atoms.

Proof. Follows directly from condition (34), observation that $\mu_0(j, m) + \mu_1(j, m) = 2^{j-1} - 1$ and $\chi_{\pm 2^{j-1}(m+1)} \cap \chi_{\pm 2^{j-1}m}$ has no integer points. \square

In addition, we would like the discrete wave atom transform to be a unitary operator. This requires special treatment of the lowest and highest frequencies, corresponding to the left-most and right-most wave packets in the tree T . So we define a modified basis $\{\tilde{\psi}_m^j\}$ as follows: we straighten the rightmost wave packet corresponding to $W_{m_r}^{j_r} \in \Lambda_T$ as its support extends beyond the interval of interest $\{-N/2, \dots, N/2 - 1\}$. Moreover, we also modify the wave packet corresponding to the leftmost leaf node $W_0^{j_l} \in \Lambda_T$ as its support approaches the origin, as follows:

$$\tilde{\psi}_m^j(k) = \begin{cases} 2^{-j/2} e^{-i\pi 2^{-j} k} e^{(-1)^{k < 0} i \alpha_0} & \text{if } |k| \leq \mu_0(j_l, 0), W_m^j = W_0^{j_l}, \\ 2^{-j/2} e^{-i\pi 2^{-j} k} e^{(-1)^{k < 0} i \alpha_{m_r}} & \text{if } |k| > m_r 2^{j_r} + \mu_0(j_r, m_r), W_m^j = W_{m_r}^{j_r}, \\ \hat{\psi}_m^j(k) & \text{otherwise.} \end{cases} \quad (35)$$

Similarly to equation (7), we then define wave atoms with the shift of $2^{-j}n$ in the spatial domain to be

$$\tilde{\psi}_{m,n}^j(k) = e^{-i2\pi n 2^{-j} k} \tilde{\psi}_m^j(k). \quad (36)$$

An example of this construction is shown on Figure 9. Now, we can formally define the quantum wave atom transform.

Definition 4. Consider a wave atom admissible tree T with a root node W_0^L . Define a matrix C^A as

$$C_{m2^j+n,i}^A = \overline{\tilde{\psi}_{m,n}^j(d(i))}, \quad (37)$$

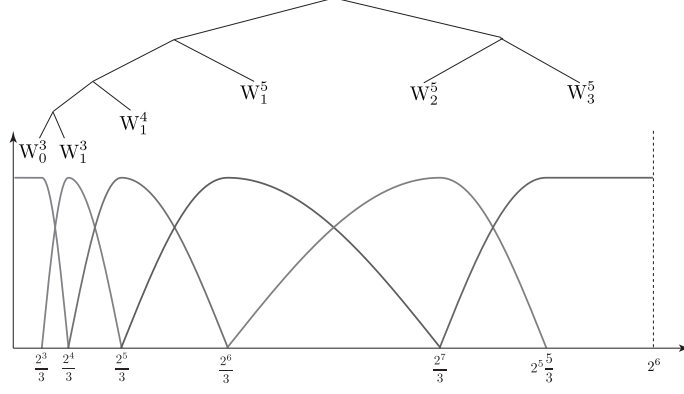


Fig. 9 Wave atoms $\tilde{\psi}_m^j$ corresponding to the wave atom admissible tree on the top (absolute values). The figure shows only the positive side of the frequency domain. The negative side of the frequency domain is symmetric.

where $W_m^j \in \Lambda_T$, d is the decoding function in equation (19), and $n, i \in \mathbb{Z}$ such that $0 \leq n < 2^j$ and $0 \leq i < N$. The following transform of size $N = 2^L$, where Q_L is QFT,

$$\sum_{k=0}^{N-1} f[k] |k\rangle \mapsto \sum_{W_m^j \in \Lambda_T} \sum_{n=0}^{2^j-1} \left(\sum_{i=0}^{N-1} C_{m2^j+n,i}^A \hat{f}[d(i)] \right) |m2^j + n\rangle \quad (38)$$

$$\text{where } \hat{f}[k] = \begin{cases} \sum_{i=0}^{N-1} (Q_L^\dagger)_{ki} f[i], & \text{if } k \geq 0, \\ \sum_{i=0}^{N-1} (Q_L^\dagger)_{(k+N)i} f[i], & \text{if } k < 0, \end{cases}$$

is called a quantum wave atom transform.

5.3 Decomposition of C^A

Recall that the Shannon wavelet transform was implemented using a Fourier-like transform that had a block-diagonal structure determined by the wave packet tree T (see Section 4). To implement the wave atom transform, one can use the same idea, combined with a new technique: redistribution of weights between elements of the vector \hat{f} , sometimes called “blending” [22]. This is needed because of the overlaps between the supports of neighboring wave atoms over the frequency domain (which did not occur in the case of Shannon wavelets).

In this section, we will decompose the matrix C^A (from Definition 4) into a product of a blending operation, and a Fourier-like transform.

Classically, for a given node W_m^j in the tree T , the wave atom transform blends 2^j pairs of elements of the vector \hat{f} into a vector of size 2^j and applies the Fourier transform of size 2^j to obtain the vector of wave atom coefficients $\{c_{j,m,n}^D\}_{n=0}^{2^j-1}$ [9]. Unless we consider border cases of W_m^j , the transform blends $\hat{f}[k]$ and $\hat{f}[k']$, for all

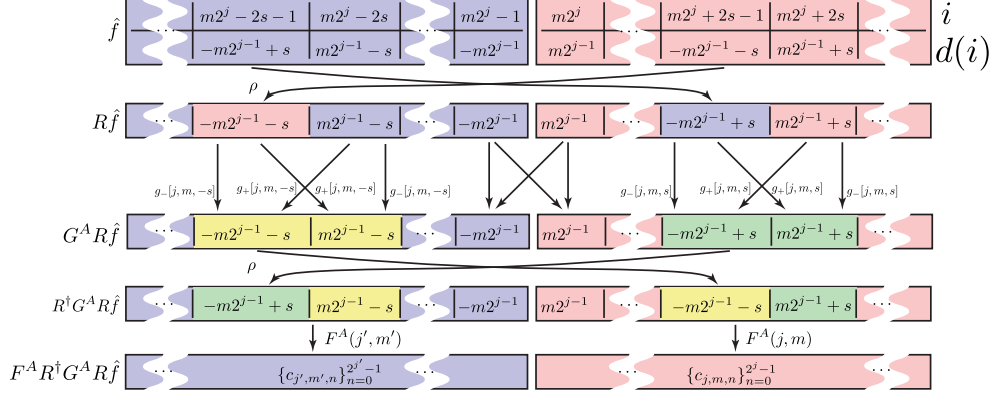


Fig. 10 The decomposition of the wave atom transform starting from the state of $\sum_{k=0}^{N-1} \hat{f}[d(k)] |k\rangle$. We illustrate the blending in the intervals $\chi_{\pm m2^j}$ that represent the intersection of supports of two wave atoms: $W_{m'}^{j'}$ on the left side and W_m^j on the right side.

pairs (k, k') of the form:

$$\begin{aligned} &(-m2^{j-1} + s, m2^{j-1} + s), \quad \forall |s| \leq \mu_0(j, m), \\ &(-(m+1)2^{j-1} + s, (m+1)2^{j-1} + s), \quad \forall |s| \leq \mu_1(j, m). \end{aligned}$$

(This can be seen by recalling Definition 4, equations (35)-(36), and the fact that $\hat{\psi}_m^j$ is supported on two intervals in the frequency domain, as in equation (30).)

In order to implement the blending efficiently, we permute elements of the vector \hat{f} such that the pairs involved in the blending become adjacent to each other. Given that the encoding procedure (18) orders frequencies by increasing absolute values, for some W_m^j and $|s| \leq \mu_0(j, m)$, the pair of frequencies $-m2^{j-1} + s$ and $m2^{j-1} + s$ are not neighboring indices when encoded unless $s = 0$. Therefore, the blending procedure becomes a three-stage process.

1. Permute elements of the vector \hat{f} such that $-m2^{j-1} + s$ and $m2^{j-1} + s$ become neighbors by swapping $-m2^{j-1} + s$ with $-m2^{j-1} - s$.
2. Redistribute the weights between adjacent elements according to the function g .
3. Reverse the permutation in Step 1.

Figure 10 schematically illustrates the decomposition of C^A by tracking the actions on pairs $\pm m2^{j-1} \pm s$. In the following, we define the building blocks that are used to construct C^A .

Definition 5. For each $W_m^j \in \Lambda_T$, consider matrix $F^A(j, m) \in \mathbb{C}^{2^j \times 2^j}$ defined by elements

$$(F^A(j, m))_{n,c} = 2^{-j/2} e^{i2\pi 2^{-j}(n+\frac{1}{2})d(m2^j+c)} e^{(-1)^{c+1}i\alpha_m}, \quad \text{for } 0 \leq n, c < 2^j. \quad (39)$$

Let us define matrix $F^A \in \mathbb{C}^{N \times N}$ of Fourier transform adapted to tree structure of T as a composition of matrices $F^A(j, m)$,

$$F^A = \bigoplus_{W_m^j \in \Lambda_T} F^A(j, m), \quad (40)$$

that is to say,

$$F_{m2^j+n, m2^j+c}^A = (F^A(j, m))_{n,c}, \text{ for } W_m^j \in \Lambda_T, 0 \leq n, c < 2^j. \quad (41)$$

Definition 6. Let us define permutation of indices $\rho : \{0, \dots, N-1\} \mapsto \{0, \dots, N-1\}$ by its non-trivial actions as

$$\forall W_m^j \in \Lambda_T \text{ s.t. } W_m^j \neq W_0^{j_i}, \forall |s| \leq \mu_0(j, m), \rho(m2^j + 2s - 1) = m2^j - 2s - 1. \quad (42)$$

Define its permutation matrix $R \in \mathbb{C}^{N \times N}$ such that nonzero elements of the matrix are

$$R_{\rho(i)i} = 1 \text{ for } i \in \{0, \dots, N-1\}.$$

Let us use the following shorthand for function g . For $j \geq 1, m \geq 0$ and $s \in \mathbb{Z}$,

$$\begin{aligned} g_-[j, m, s] &= g((-1)^m (2^{-j+1} \pi |s| - \frac{\pi}{2})), \\ g_+[j, m, s] &= \mathbf{i}(-1)^{I(s < 0)} g((-1)^{m+1} (2^{-j+1} \pi |s| + \frac{\pi}{2})). \end{aligned} \quad (43)$$

Definition 7. Let us define blending matrix $G^A \in \mathbb{C}^{N \times N}$ as follows: for any $W_m^j \in \Lambda_T$ such that $W_m^j \neq W_0^{j_i}$, and for any $s \in \mathbb{Z}$ such that $|s| \leq \mu_0(j, m)$,

$$\begin{pmatrix} G_{m2^j+2s-1, m2^j+2s-1}^A & G_{m2^j+2s-1, m2^j+2s}^A \\ G_{m2^j+2s, m2^j+2s-1}^A & G_{m2^j+2s, m2^j+2s}^A \end{pmatrix} = \begin{pmatrix} g_-[j, m, s] & g_+[j, m, s] \\ g_+[j, m, s] & g_-[j, m, s] \end{pmatrix}, \quad (44)$$

and G^A is the identity on other diagonal blocks.

Theorem 5. The matrix C^A (from Definition 4) is a product of matrices given by Definitions 5, 6, 7,

$$C^A = F^A R^\dagger G^A R. \quad (45)$$

Proof. See Appendix B.4. \square

Corollary 6. The matrix C^A is unitary.

Proof. This follows from the observation that each matrix in the product of equation (45) is unitary. The blocks of G^A are unitary due to properties (9) and (10) of the function g . \square

In the following subsections, we discuss the implementation of each of the operators, F^A , G^A and R .

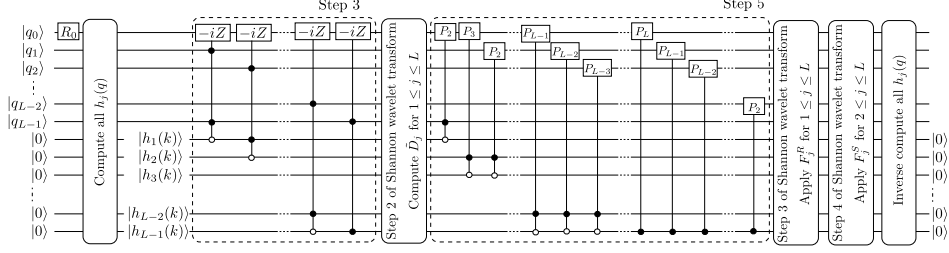


Fig. 11 Quantum circuit implementation of Fourier transform adaptive to tree structure for the wave atom transform, F^A of size 2^L . Steps 2-4 of the Shannon wavelet transform can be found on Figure 7 or in Algorithm 4.

5.4 Quantum implementation of F^A

In this section we will implement the operation F^A defined in (39), for a variety of wave packet trees T . This is similar to the implementation of the Shannon wavelet transform in (28), modulo some technical details.

First, equation (39) involves a complex phase factor that has a periodicity of 2^{j+1} (rather than 2^j , in the case of (28)):

$$e^{i2^{-j}2\pi(n+\frac{1}{2})d(m2^j+c)} = e^{i2^{-j}2\pi(n+\frac{1}{2})(d(m2^j+c)+p2^{j+1})}.$$

Recall that in the wave packet encoding (22), the j least significant bits represent c in binary form while the remaining bits represent m . So the $(j+1)$ -th bit represents the parity of m , which determines the shape of the wavepacket (see Section 2.2).

Recall functions d and \tilde{d} defined by (19), (21) correspondingly and observe that

$$d(m2^j + c) = \tilde{d}(c, j, m) + (-1)^c \lfloor \frac{m}{2} \rfloor \cdot 2^j - I(c \text{ is odd}) \cdot 2^j. \quad (46)$$

Like in the case of Shannon wavelets, the decoding \tilde{d} keeps us within the same block of size 2^j . However, (46) shows that some adjustment is required due to the change in periodicity. Then, each block of the matrix F^A can be expressed as the product of three factors:

$$(F^A(j, m))_{n,c} = \underbrace{e^{(-1)^c i\pi \lfloor \frac{m}{2} \rfloor} e^{-I(c \text{ is odd}) i\pi} e^{(-1)^{c+1} i\alpha_m}}_{r_m} \underbrace{e^{i\pi 2^{-j} \tilde{d}(c, j, m)}}_{\text{Phase}} \underbrace{2^{-j/2} e^{i\pi 2^{-j} n \cdot \tilde{d}(c, j, m)}}_{\text{QFT}}. \quad (47)$$

The first factor of (47) represents the necessary adjustment. Consider combination of values of c and m :

$$r_m(c) = \begin{cases} e^{-i\pi/4} & \text{if } m = c \bmod 2, \\ -e^{i\pi/4} & \text{if } m \neq c \bmod 2. \end{cases} \quad (48)$$

For quantum realization, we would like to have a unitary corresponding different cases of m and c . We may apply the following operators to the qubit corresponding to the

least significant bit of c which defines its parity.

$$R_0 = \begin{pmatrix} e^{-i\pi/4} & 0 \\ 0 & -e^{i\pi/4} \end{pmatrix}, \quad R_1 = R_0 \cdot (-iZ). \quad (49)$$

We apply R_0 if m is even and R_1 if m is odd.

The complete procedure is described in Appendix A.2 (Algorithm 5), with its circuit shown in Figure 11. The gate complexity of the algorithm is $O(L^2)$.

5.5 Quantum implementation of G^A

Recall Definition 7, where each block of matrix G^A is defined by equation (44). It will be convenient to shift the indices of this matrix by 1. In other words, let us define the block-diagonal matrix $\tilde{G}^A \in \mathbb{C}^{N \times N}$ as follows: for $W_m^j \neq W_0^j$ and $|s| \leq \mu_0(j, m)$,

$$\begin{pmatrix} \tilde{G}_{m2^j+2s, m2^j+2s}^A & \tilde{G}_{m2^j+2s, m2^j+2s+1}^A \\ \tilde{G}_{m2^j+2s+1, m2^j+2s}^A & \tilde{G}_{m2^j+2s+1, m2^j+2s+1}^A \end{pmatrix} = \begin{pmatrix} g_-[j, m, s] & g_+[j, m, s] \\ g_+[j, m, s] & g_-[j, m, s] \end{pmatrix}. \quad (50)$$

This satisfies

$$G^A = \text{Adder}_L(1) \tilde{G}^A \text{Adder}_L(-1),$$

where $\text{Adder}_L(\pm 1)$ is the unitary operation defined in equation (3).

Furthermore, the definition of \tilde{G}^A involves both positive and negative shifts s from $m2^j$. The challenge with this approach is that when we work with wave packets in W_m^j , it requires knowing information about the left neighbor of W_m^j in the tree. It would be more practical if we could define the operation \tilde{G}^A in a way that involves only positive shifts (which we denote by n), and only one leaf node W_m^j at a time. This can be done in the following way.

We can re-write the formula (50) for \tilde{G}^A in terms of $n \in \{0, \dots, 2^{j-1} - 1\}$ for $W_m^j \in \Lambda_T$. Then for $W_m^j \neq W_0^j$ and $0 \leq n \leq \mu_0(j, m)$, we have the same expressions as in (50), but substituting $s \mapsto n$:

$$\begin{aligned} \tilde{g}_-^{(0)}[j, m, n] &= g \left((-1)^m \pi (2^{-j+1}n - \tfrac{1}{2}) \right), \\ \tilde{g}_+^{(0)}[j, m, n] &= \mathbf{i}g \left((-1)^{m+1} \pi (2^{-j+1}n + \tfrac{1}{2}) \right), \\ \begin{pmatrix} \tilde{G}_{m2^j+2n, m2^j+2n}^A & \tilde{G}_{m2^j+2n, m2^j+2n+1}^A \\ \tilde{G}_{m2^j+2n+1, m2^j+2n}^A & \tilde{G}_{m2^j+2n+1, m2^j+2n+1}^A \end{pmatrix} &= \begin{pmatrix} \tilde{g}_-^{(0)}[j, m, n] & \tilde{g}_+^{(0)}[j, m, n] \\ \tilde{g}_+^{(0)}[j, m, n] & \tilde{g}_-^{(0)}[j, m, n] \end{pmatrix}, \end{aligned} \quad (51)$$

and for $W_m^j \neq W_{m_r}^j$ and $\mu_0(j, m) < n < 2^{j-1}$, we have the same expressions as in (50), but substituting $(j, m) \mapsto (j, m+1)$ and $s \mapsto n - 2^{j-1}$:

$$\begin{aligned} \tilde{g}_-^{(1)}[j, m, n] &= g \left((-1)^m \pi (2^{-j+1}n - \tfrac{1}{2}) \right), \\ \tilde{g}_+^{(1)}[j, m, n] &= -\mathbf{i}g \left((-1)^{m+1} \pi (2^{-j+1}n - \tfrac{3}{2}) \right), \\ \begin{pmatrix} \tilde{G}_{m2^j+2n, m2^j+2n}^A & \tilde{G}_{m2^j+2n, m2^j+2n+1}^A \\ \tilde{G}_{m2^j+2n+1, m2^j+2n}^A & \tilde{G}_{m2^j+2n+1, m2^j+2n+1}^A \end{pmatrix} &= \begin{pmatrix} \tilde{g}_-^{(1)}[j, m, n] & \tilde{g}_+^{(1)}[j, m, n] \\ \tilde{g}_+^{(1)}[j, m, n] & \tilde{g}_-^{(1)}[j, m, n] \end{pmatrix}. \end{aligned} \quad (52)$$

So far, the discussion of wave atoms did not rely on the exact form of function g . Each block of matrix \tilde{G}^A depends on the value of $2^{-j+1}n$, and there are $O(2^{j_m})$ distinct such values, where j_m is the maximum level of leaf nodes in the tree. Therefore there are $O(2^{j_m})$ different types of blocks in \tilde{G}^A . So, in the general case, the number of gates in the implementation of \tilde{G}^A without any approximation is $O(2^{j_m})$. However, the complexity can be reduced for certain choices of the function g .

5.5.1 Efficient implementation of \tilde{G}^A

We give an example of a function g for which \tilde{G}^A can be implemented exactly and efficiently. Consider the following function g :

$$g(w) = \begin{cases} \cos(\frac{3}{8}w - \frac{\pi}{16}), & \text{if } -\frac{7}{6}\pi \leq w \leq \frac{\pi}{6}, \\ \cos(\frac{3}{4}w - \frac{\pi}{8}), & \text{if } \frac{\pi}{6} < w \leq \frac{5}{6}\pi, \\ 0, & \text{otherwise.} \end{cases} \quad (53)$$

This is a simple example of a function that resembles an asymmetric “bump” and satisfies the requirements in equation (9) and equation (10). Other types of functions satisfying these requirements also can be considered.

For this choice of g , let

$$v(j, m, n) = \begin{cases} \frac{\pi}{2^{j+2}} (3n - 2^{j-1}) \cdot 2^{I(n \leq \mu_0(j, m))}, & \text{if } m \text{ is odd,} \\ \frac{\pi}{2^{j+2}} (3n - 2^j) \cdot 2^{I(n > \mu_0(j, m))}, & \text{if } m \text{ is even,} \end{cases} \quad (54)$$

then

$$\begin{aligned} \begin{pmatrix} \tilde{G}_{m2^j+2n, m2^j+2n}^A & \tilde{G}_{m2^j+2n, m2^j+2n+1}^A \\ \tilde{G}_{m2^j+2n+1, m2^j+2n}^A & \tilde{G}_{m2^j+2n+1, m2^j+2n+1}^A \end{pmatrix} &= \begin{pmatrix} \cos(v(j, m, n)) & \mathbf{i} \sin(v(j, m, n)) \\ \mathbf{i} \sin(v(j, m, n)) & \cos(v(j, m, n)) \end{pmatrix} \\ &= S^\dagger \underbrace{\begin{pmatrix} \cos(v(j, m, n)) & \sin(v(j, m, n)) \\ -\sin(v(j, m, n)) & \cos(v(j, m, n)) \end{pmatrix}}_{\text{Linear Pauli Rotations}} S, \end{aligned} \quad (55)$$

where S denotes the single-qubit gate $S = \begin{pmatrix} 1 & 0 \\ 0 & \mathbf{i} \end{pmatrix}$.

The middle factor in (55) can be implemented, by using the formulas (54), and applying a controlled single-qubit gate of the form

$$|x\rangle |y\rangle \mapsto |x\rangle \left(\cos(ax + b) |y\rangle + (-1)^y \sin(ax + b) |y \oplus 1\rangle \right), \text{ for } y \in \{0, 1\}, \quad (56)$$

which we call a “linear Pauli rotation” with slope $2a$ and offset $2b$. This can be implemented using the quantum circuit shown in Figure 12. This procedure is described in detail in Appendix A.2 (Algorithm 6), and has gate complexity of $O(L^2)$.

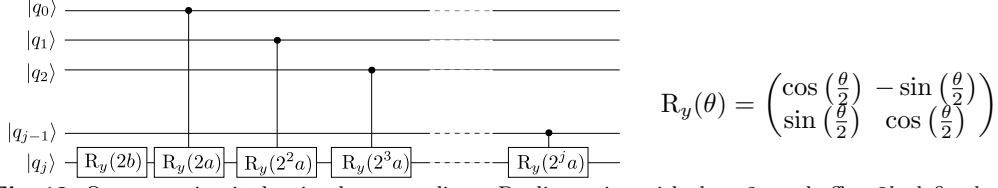


Fig. 12 Quantum circuit that implements a linear Pauli rotation with slope $2a$ and offset $2b$, defined in equation (56).

Finally, to implement \tilde{G}^A , we need to call Algorithm 6 controlled by the predicates $I(q > 2\mu_0(j_l, 0))$ and $I(q \leq m_r 2^{j_r} + 2\mu_0(j_r, m_r))$.

5.6 Quantum implementation of R

Recall that, by Definition 6, the action of R is described by a permutation ρ , and ρ permutes odd indices as follows. For any $W_m^j \neq W_0^{j_l}$ and $s \in \mathbb{Z}$ such that $|s| \leq \mu_0(j, m)$,

$$\rho(m2^j + 2s - 1) = m2^j - 2s - 1.$$

Let us exclude even indices from consideration. We identify the set of odd indices $\{1, 3, 5, \dots, N-1\}$ with the set of all indices up to $N/2-1$, that is $\{0, 1, 2, \dots, N/2-1\}$. We let $\dot{\rho}$ denote the permutation acting on $\{0, 1, 2, \dots, N/2-1\}$ that corresponds to ρ .

For a fixed leaf node W_m^j such that $W_m^j \neq W_0^{j_l}$, let us denote the permutation associated with leaf node W_m^j by $\dot{\rho}_m^j$. Then $\dot{\rho}_m^j$ has non-trivial action as

$$\dot{\rho}_m^j(m2^{j-1} + s) = m2^{j-1} - s \text{ for } s \in \mathbb{Z} \text{ s.t. } |s| \leq \mu_0(j, m). \quad (57)$$

Combining all permutations $\dot{\rho}_m^j$ together we get the permutation $\dot{\rho}$, which is connected to ρ as follows:

$$\dot{\rho} = \prod_{W_m^j \neq W_0^{j_l}} \dot{\rho}_m^j, \quad (58)$$

$$\rho(2k-1) = 2\dot{\rho}(k) - 1. \quad (59)$$

The order in the product is not important since all permutations $\dot{\rho}_m^j$ generated by wave atom admissible tree T pair-wise commute. This follows from the observation that no two such permutations have non-trivial action on the same index. One can notice that equation (59) does not work in case of $k = N/2$ or $k = 0$. However, ρ and $\dot{\rho}$ act trivially on the boundaries, so we do not consider such k 's.

Each $\dot{\rho}_m^j$ acts non-trivially on $2\mu_0(j, m)$ indices. Let us combine permutations that share the same value of $2\mu_0(j, m)$. Suppose this common value is $2\mu_0(j_*, 0)$, for some j_* . Then let $\dot{\rho}^{j_*}$ denote the combined permutation. By the definition of μ_0 in equation (33),

$$\dot{\rho}^{j_*} = \prod_{\substack{W_m^j \neq W_0^{j_l} \\ \mu_0(j, m) = \mu_0(j_*, 0)}} \dot{\rho}_m^j = \prod_{\substack{W_m^j \neq W_0^{j_l} \\ j - I(m \text{ is odd}) = j_*}} \dot{\rho}_m^j. \quad (60)$$

Algorithm 3 Applying permutation $\dot{\rho}^{j*}$, given values of helper function $h_{j*}^\rho(\cdot)$

Input: $\sum_{q=0}^{2^{L-1}-1} \alpha_q |q\rangle |h_{j*}^\rho(q)\rangle$, that is, a superposition over indices $|q\rangle$, with labels $|h_{j*}^\rho(q)\rangle$ computed by the helper function $h_{j*}^\rho(\cdot)$.

Result: $\sum_{q=0}^{2^{L-1}-1} \alpha_q |\dot{\rho}^{j*}(q)\rangle |h_{j*}^\rho(q)\rangle$.

Notation:

Quantum register \mathcal{R}_q of $L-1$ qubits; $\mathcal{R}_q[i]$ denotes the i -th qubit, $i = 0, \dots, L-1$;

Quantum register \mathcal{R}_h of 1 qubit.

1. Apply $\text{Adder}_{L-1}(\mu_0(j*, 0))$ to \mathcal{R}_q controlled on $\mathcal{R}_h = |1\rangle$.
 2. For each $i = 0, \dots, j*-2$ apply X -gate to $\mathcal{R}_q[i]$ controlled on $\mathcal{R}_h = |1\rangle$.
 3. Apply $\text{Adder}_{L-1}(-\mu_1(j*, 0))$ to \mathcal{R}_q controlled on $\mathcal{R}_h = |1\rangle$.
-

For permutation ρ , let us define a helper function $\tilde{h}^\rho : \{0, \dots, N/2 - 1\} \mapsto \{0, \dots, L-2\}$ that says, for each index, which permutation $\dot{\rho}^{j*}$ acts nontrivially on it. Formally, we have:

$$\begin{aligned} \forall W_m^j \neq W_0^{j_l} \text{ and } |s| \leq \mu_0(j, m), \quad \tilde{h}^\rho(m2^{j-1} + s) = j - I(m \text{ is odd}), \\ \tilde{h}^\rho(k) = 0 \text{ if } k \leq \mu_0(j_l, 0) \text{ or } k > m_r 2^{j_r-1} + \mu_0(j_r, m_r). \end{aligned} \quad (61)$$

For $j \in \{1, \dots, L-1\}$ define a family of boolean functions $h_j^\rho : \{0, \dots, N/2 - 1\} \mapsto \{0, 1\}$ such that

$$h_j^\rho(k) = I(h^\rho(k) = j). \quad (62)$$

With such boolean helper functions, the quantum implementation of $\dot{\rho}^{j*}$ in equation (60) becomes a three-stage process listed in Algorithm 3. One can notice that $\dot{\rho}$ keeps indices within their respective intervals centered around $m2^{j-1}$ for some W_m^j . This means that

$$\tilde{h}^\rho(k) = \tilde{h}^\rho(\dot{\rho}(k)) \text{ for any } k \in \{0, \dots, N/2 - 1\}, \quad (63)$$

which implies that the calculation of h_j^ρ 's can be reversed after $\dot{\rho}$ is applied.

Finally, we show a way to compute the helper functions $h_j^\rho(\cdot)$, using the helper functions $h_j(\cdot)$ defined in (24). We start by examining a leaf node $W_m^j \notin \{W_0^{j_l}, W_{m_r}^{j_r}\}$. Consider an index $m2^{j-1} + n$ where $n \in \{0, \dots, N/2 - 1\}$. There are two cases:

- If $n \leq \mu_0(j, m)$, then $\tilde{h}^\rho(m2^{j-1} + n) = j - I(m \text{ is odd})$ as $m2^{j-1} + n$ is affected by the permutation $\dot{\rho}_m^j$.
- If $n > \mu_0(j, m)$, then $\tilde{h}^\rho(m2^{j-1} + n) = j - I(m \text{ is even})$ as $m2^{j-1} + n$ is affected by the permutation $\dot{\rho}_{m'}^{j'}$, where $W_{m'}^{j'}$ is the right neighbor of W_m^j .

For $W_m^j \in \{W_0^{j_l}, W_{m_r}^{j_r}\}$, in one of the above cases $\tilde{h}^\rho(m2^{j-1} + n) = 0$ according to the definition in equation (61). Finally, one can evaluate these expressions, by obtaining the value of j from the functions $h_j(\cdot)$.

The above procedure is described in Appendix A.2 (Algorithm 7). Its gate complexity is $O(L^2)$.

Together, the complexity of implementation of the permutation $\dot{\rho}$ is $O(L^2)$, given that we need to call Algorithm 7 two times to compute and reverse h_j^ρ 's, and call $O(L)$ times Algorithm 3 (we care about $2 \leq j < L$).

Finally, one can implement the operation R (i.e., the permutation ρ) as follows: given that

$$\rho(2k+1) = \rho(2(k+1)-1) = 2\dot{\rho}(k+1) - 1,$$

the implementation of R consists of: a shift by 2; the circuit that implements $\dot{\rho}$ on qubits $1, \dots, L-1$, controlled by the parity of qubit 0; and a shift by -2 . This transforms the initial state of $|2k+1\rangle$ into $|2(k+1)+1\rangle$; then the state after applying $\dot{\rho}$ is $|2\dot{\rho}(k+1)+1\rangle$, which we need to transform into $|2\dot{\rho}(k+1)-1\rangle$.

5.7 Computational Complexity

The classical complexity of the 1-D wave atom transform is the same as the complexity of the fast Fourier transform $O(N \log N)$ where N is the number of points in discretization [9].

The quantum implementation of the wave atom transform that combines all the steps in decomposition

$$C^A = F^A R^\dagger G^A R,$$

depends on

1. Efficient computation of the family of boolean functions $h_j(\cdot), j = \{1, \dots, L-1\}$ for tree T ,
2. Efficient computation of blocks of G^A .

Here, efficient computation means polynomial time in the number of qubits, in other words, polylogarithmic in N . The results are summarized in the following theorem.

Theorem 7 (Quantum complexity of 1D wave atom transform). *Take a wave atom admissible tree T defined for discretization of size $O(2^L)$. If*

- *function g of the wave atom transform allows the implementation of matrix G^A with gate complexity of $O(L^2)$,*
- *the family of functions $h_j(\cdot)$ has a quantum implementation that requires $O(L^2)$ gates,*

then the gate complexity of quantum wave atom transform generated by tree T and function g is $O(L^2)$.

In section 5.5, we provided a concrete implementation of the matrix G^A for a specific function g . In addition, recall from section 3.2 that the family of functions h_j can be efficiently implemented for monotonic trees. This implies the following corollary.

Corollary 8 (Quantum complexity of 1D wave atom transform for monotonic trees). *Let T be a monotonic wave atom admissible tree defined for discretization of size $O(2^L)$. If T is represented by the leftmost node on each level, then the gate complexity*

of the quantum wave atom transform generated by the tree T and the function g defined in (53) is $O(L^2)$. The complexity of the construction of the quantum circuit is $O(L^2)$.

6 Discussion

The first result of this paper is a quantum implementation of Shannon wavelet transform with a hierarchical tree structure of shifts and scales (Theorem 2). This construction made use of helper decoding functions $h_j(\cdot)$ (equation (24)) that map indices to their respective levels in the wave packet tree. With such functions, the hierarchical quantum Shannon wavelet transform becomes a product of Fourier transforms of different scales. The type of wave packet trees dictates the circuit implementation of functions h_j . We demonstrated that for monotonic trees, the implementation of helper decoding functions is efficient and requires $O(L^2)$ gates, when implementing a wavelet transform of dimension 2^L . Together, this allows us to achieve exponential speedup with the quantum gate complexity of $O(L^2)$ for the entire procedure of Shannon wavelet transform.

The wave atom transform with a hierarchical tree structure is more intricate as it requires “blending” [22], due to the overlaps between the supports of neighboring wave packets in frequency space [9, 11]. A crucial contribution of this paper is to show how to implement blending that *also follows the tree structure*, on a quantum computer, i.e., acting on quantum superposition states. Using this technique, we showed that for monotonic admissible trees with wave atoms satisfying some technical conditions, the quantum wave atom transform also achieves an exponential speedup with the gate complexity of $O(L^2)$ (Theorem 7). We demonstrated this exponential speedup for wave atoms constructed from a particular function $g(\cdot)$ (Corollary 8). In particular, this family of wave atoms has “parabolic scaling,” which is useful for constructing sparse representations of solutions to wave equations [9]. Generalizing this construction is an interesting topic for future work.

Using tree-structured wavelet bases, one has additional flexibility to construct wavelet bases with desirable properties. This suggests considering other wave packet trees that satisfy our admissibility conditions (Definition 3). However, one is unlikely to find a single “universal” quantum algorithm that is efficient and applicable to all admissible trees. The general tree representation requires at least $O(2^L)$ bits as there are more than $2^{2^{L-1}}$ different admissible wave packet trees [4]. If there is a classical step, the decoding of the tree representation is already $\Omega(2^L)$.

Another potential future direction involves higher-dimensional wave packet transforms, which could help solve wave equations and systems of hyperbolic differential equations in general, as its basis offers a sparse representation of the solution operator [8, 10, 12, 13]. This paper shows a 1-dimensional wave atom transform, which can be extended to construct a multi-dimensional transform. For example, taking products of 1-D wavelet packets allows for constructing two-dimensional orthonormal basis functions with four bumps in the frequency plane. Although the construction is not a straightforward tensor product since both dimensions share the same scale [8], the results in 1-D are easily extendable to the 2-D case.

Acknowledgements: MP is grateful to Radu Balan for the discussion related to this paper, which restored belief in the best.

This work is supported by a collaboration between the US DOE and other Agencies. This material is based upon work supported by the U.S. Department of Energy, Office of Science, Accelerated Research in Quantum Computing, Fundamental Algorithmic Research toward Quantum Utility (FAR-Qu). Additional support is acknowledged from NSF and NIST.

MP also acknowledges funding and support from a NIST/UMD Joint Center for Quantum Information and Computer Science (QuICS) Lanczos Graduate Fellowship, and a MathQuantum Graduate Fellowship (NSF award DMS-2231533).

Contributions by NIST employees are not subject to US copyright protection.

References

- [1] Jozsa, R.: Quantum algorithms and the fourier transform. Proceedings of the Royal Society of London. Series A: Mathematical, Physical and Engineering Sciences **454**(1969), 323–337 (1998) <https://doi.org/10.1098/rspa.1998.0163>
- [2] Childs, A.M., Van Dam, W.: Quantum algorithms for algebraic problems. Reviews of Modern Physics **82**(1), 1–52 (2010)
- [3] Daubechies, I.: Ten Lectures on Wavelets. Society for Industrial and Applied Mathematics, USA (1992)
- [4] Mallat, S.: A Wavelet Tour of Signal Processing, Third Edition: The Sparse Way, 3rd edn. Academic Press, Inc., USA (2008)
- [5] Daubechies, I.: Orthonormal bases of compactly supported wavelets II. variations on a theme. SIAM J. Math. Anal. **24**(2), 499–519 (1993)
- [6] Ryan, H.: Ricker, ormsby, klander, butterworth – a choice of wavelets. CSEG Recorder **19**(7), 8–9 (1994)
- [7] Gabor, D.: Theory of communication. part 1: The analysis of information. Journal of the Institution of Electrical Engineers - Part III: Radio and Communication Engineering **93**(26), 429–441 (1946) <https://doi.org/10.1049/ji-3-2.1946.0074>
- [8] Demanet, L.: Curvelets, wave atoms, and wave equations. PhD thesis (2006). <https://doi.org/10.7907/1TEF-RQ51> . <https://resolver.caltech.edu/CaltechETD:etd-05262006-133555>
- [9] Demanet, L., Ying, L.: Wave atoms and sparsity of oscillatory patterns. Applied and Computational Harmonic Analysis **23**(3), 368–387 (2007) <https://doi.org/10.1016/j.acha.2007.03.003>
- [10] Demanet, L., Ying, L.: Wave atoms and time upscaling of wave equations. Numer. Math. (Heidelb.) **113**(1), 1–71 (2009)

- [11] Villemoes, L.F.: Wavelet packets with uniform time-frequency localization. *Comptes Rendus Mathématique* **335**, 793–796 (2002)
- [12] Candes, E.J., Demanet, L.: The curvelet representation of wave propagators is optimally sparse. *Communications on Pure and Applied Mathematics* **58**(11), 1472–1528 (2005)
- [13] Candès, E., Demanet, L.: Curvelets and fourier integral operators. *C. R. Math. Acad. Sci. Paris* **336**(5), 395–398 (2003)
- [14] Demanet, L., Létourneau, P.-D., Boumal, N., Calandra, H., Chiu, J., Snelson, S.: Matrix probing: A randomized preconditioner for the wave-equation hessian. *Applied and Computational Harmonic Analysis* **32**, 155–168 (2012) <https://doi.org/10.1016/j.acha.2011.03.006>
- [15] Harrow, A.W., Hassidim, A., Lloyd, S.: Quantum algorithm for linear systems of equations. *Physical Review Letters* **103**(15) (2009) <https://doi.org/10.1103/physrevlett.103.150502>
- [16] Morales, M.E., Pira, L., Schleich, P., Koor, K., Costa, P., An, D., Aspuru-Guzik, A., Lin, L., Rebentrost, P., Berry, D.W.: Quantum linear system solvers: A survey of algorithms and applications. *arXiv preprint arXiv:2411.02522* (2024)
- [17] Berry, D.W.: High-order quantum algorithm for solving linear differential equations. *Journal of Physics A: Mathematical and Theoretical* **47**(10), 105301 (2014)
- [18] Childs, A.M., Maslov, D., Nam, Y., Ross, N.J., Su, Y.: Toward the first quantum simulation with quantum speedup. *Proceedings of the National Academy of Sciences* **115**(38), 9456–9461 (2018)
- [19] Jennings, D., Lostaglio, M., Lowrie, R.B., Pallister, S., Sornborger, A.T.: The cost of solving linear differential equations on a quantum computer: fast-forwarding to explicit resource counts. *Quantum* **8**, 1553 (2024)
- [20] Clader, B.D., Jacobs, B.C., Sprouse, C.R.: Preconditioned quantum linear system algorithm. *Physical review letters* **110**(25), 250504 (2013)
- [21] Berry, D.W., Childs, A.M., Cleve, R., Kothari, R., Somma, R.D.: Exponential improvement in precision for simulating sparse hamiltonians. In: *Proceedings of the Forty-sixth Annual ACM Symposium on Theory of Computing*, pp. 283–292 (2014)
- [22] Ni, H., Ying, L.: Quantum wave packet transforms with compact frequency support (2024). <https://arxiv.org/abs/2405.00929>
- [23] Costa, P.C., Jordan, S., Ostrander, A.: Quantum algorithm for simulating the

- wave equation. *Physical Review A* **99**(1), 012323 (2019)
- [24] Hoyer, P.: Efficient Quantum Transforms (1997). <https://arxiv.org/abs/quant-ph/9702028>
 - [25] Fijany, A., Williams, C.P.: Quantum Wavelet Transforms: Fast Algorithms and Complete Circuits (1998). <https://arxiv.org/abs/quant-ph/9809004>
 - [26] Klappenecker, A.: Wavelets and wavelet packets on quantum computers. In: Unser, M.A., Aldroubi, A., Laine, A.F. (eds.) *Wavelet Applications in Signal and Image Processing VII*. SPIE, Bellingham, WA (1999)
 - [27] Argüello, F.: Quantum wavelet transforms of any order. *Quantum Information & Computation* **9**, 414–422 (2009)
 - [28] Li, H.-S., Fan, P., Xia, H.-Y., Song, S.: Quantum multi-level wavelet transforms. *Inf. Sci. (Ny)* **504**, 113–135 (2019)
 - [29] Zhang, Z., Kon, M.A.: Wavelet matrix operations and quantum transforms. *Appl. Math. Comput.* **428**(127179), 127179 (2022)
 - [30] Bagherimehrab, M., Aspuru-Guzik, A.: Efficient quantum algorithm for all quantum wavelet transforms. *Quantum Science and Technology* **9**(3), 035010 (2024) <https://doi.org/10.1088/2058-9565/ad3d7f>
 - [31] Kiani, B.T., De Palma, G., Englund, D., Kaminsky, W., Marvian, M., Lloyd, S.: Quantum advantage for differential equation analysis. *Physical Review A* **105**(2) (2022) <https://doi.org/10.1103/physreva.105.022415>
 - [32] Bagherimehrab, M., Nakaji, K., Wiebe, N., Aspuru-Guzik, A.: Fast quantum algorithm for differential equations (2023). <https://arxiv.org/abs/2306.11802>
 - [33] Liu, Y.-K.: Quantum algorithms using the curvelet transform. In: *Proceedings of the Forty-first Annual ACM Symposium on Theory of Computing*, pp. 391–400 (2009)
 - [34] Liu, Y.-K.: An Uncertainty Principle for the Curvelet Transform, and the Infeasibility of Quantum Algorithms for Finding Short Lattice Vectors (2023). <https://arxiv.org/abs/2310.03735>
 - [35] Harrow, A.W., Recht, B., Chuang, I.L.: Efficient discrete approximations of quantum gates. *Journal of Mathematical Physics* **43**(9), 4445–4451 (2002) <https://doi.org/10.1063/1.1495899>
 - [36] Nielsen, M.A., Chuang, I.L.: *Quantum Computation and Quantum Information: 10th Anniversary Edition*. Cambridge University Press, Cambridge, UK (2010)
 - [37] Beals, R., Brierley, S., Gray, O., Harrow, A.W., Kutin, S., Linden, N., Shepherd,

- D., Stather, M.: Efficient distributed quantum computing. *Proceedings of the Royal Society A: Mathematical, Physical and Engineering Sciences* **469**(2153), 20120686 (2013) <https://doi.org/10.1098/rspa.2012.0686>
- [38] Vedral, V., Barenco, A., Ekert, A.: Quantum networks for elementary arithmetic operations. *Physical Review A* **54**(1), 147–153 (1996) <https://doi.org/10.1103/physreva.54.147>
 - [39] Cuccaro, S.A., Draper, T.G., Kutin, S.A., Moulton, D.P.: A new quantum ripple-carry addition circuit (2004). <https://arxiv.org/abs/quant-ph/0410184>
 - [40] Draper, T.G.: Addition on a Quantum Computer (2000). <https://arxiv.org/abs/quant-ph/0008033>
 - [41] Coppersmith, D.: An approximate Fourier transform useful in quantum factoring (2002). <https://arxiv.org/abs/quant-ph/0201067>
 - [42] Coifman, R.R., Meyer, Y., Wickerhauser, V.: Wavelet analysis and signal processing. In: Auslander, L., Kailath, T., Mitter, S.K. (eds.) *Signal Processing, Part I: Signal Processing Theory*, pp. 59–68. Springer, New York, NY (1990). <http://citeseer.nj.nec.com/coifman92wavelet.html>

Appendix A Quantum algorithms

A.1 Shannon wavelets

Algorithm 4 Quantum Shannon wavelet transform

Input: $|\hat{f}\rangle = \sum_{q=0}^{2^L-1} \hat{f}[d(q)] |q\rangle$.

Result: $|c^D\rangle = \sum_{W_m^j \in \Lambda_T} \sum_{n=0}^{2^j-1} \left(\sum_{q=0}^{2^L-1} \overline{\hat{\varphi}_{m,n}^j(d(q))} \hat{f}[d(q)] \right) |m2^j + n\rangle$.

Notation:

- Quantum register \mathcal{R}_q of L qubits contains the input state, $\mathcal{R}_q[i]$ corresponds to i -th qubit in register \mathcal{R}_q , $i = 0, \dots, L-1$
- Quantum register \mathcal{R}_h of $L-1$ qubits contains ancilla qubits in zero initial state with indices starting from 1, i.e., $\mathcal{R}_h[i]$ is initialized to the state $|0\rangle$, $i = 1, \dots, L-1$

1. Compute h_j , $1 \leq j < L$, by calling subroutines such that for basis state $|q\rangle$

$$\underbrace{|q\rangle}_{\mathcal{R}_q} \underbrace{|0\rangle}_{\mathcal{R}_h} \mapsto |q\rangle |h_1(q)h_2(q)\dots h_{L-1}(q)\rangle,$$

in other words, qubit $\mathcal{R}_h[i]$ is in state $|h_i(q)\rangle$.

2. For each $j = 1, \dots, L-1$ apply decoding circuit \tilde{D}_j to qubits $\mathcal{R}_q[0], \dots, \mathcal{R}_q[j]$ controlled on $\mathcal{R}_h[j] = |1\rangle$ and $\mathcal{R}_h[j+1] = |0\rangle$ (for $j = L-1$, the latter condition is omitted and \tilde{D}_j is applied to $\mathcal{R}_q[0], \dots, \mathcal{R}_q[j-1]$).
 3. For each integer j starting from $j = L$ till $j = 1$, apply QFT rotation Q_j^R to qubits $\mathcal{R}_q[0], \dots, \mathcal{R}_q[j-1]$ controlled on $\mathcal{R}_h[j] = |1\rangle$.
 4. For each $j = 2, \dots, L$ apply QFT swap Q_j^S to qubits $\mathcal{R}_q[0], \dots, \mathcal{R}_q[j-1]$ controlled on $\mathcal{R}_h[j] = |1\rangle$ and $\mathcal{R}_h[j+1] = |0\rangle$ (the latter condition is omitted for $j = L-1$).
 5. Undo the computation of step 1, returning the register \mathcal{R}_h to the state $|0\rangle$. This is feasible because the action of steps 2-4 on the register \mathcal{R}_q is block-diagonal, i.e., it preserves each subspace $\text{span}\{|q\rangle \mid \tilde{h}(q) = j\}$.
-

Proof Let us consider the evolution of $|\hat{f}\rangle$ within the subspace $\text{span}\{|q\rangle \mid \tilde{h}(q) = j\}$, in other words, the evolution of the following linear combination of the basis states

$$\sum_{\tilde{h}(q)=j} \hat{f}[d(q)] |q_{L-1}\rangle \dots |q_0\rangle |0\rangle.$$

After the first step, the state is

$$\sum_{\tilde{h}(q)=j} \hat{f}[d(q)] |q_{L-1}\rangle \dots |q_0\rangle |\underbrace{1\dots 1}_j 0\dots 0\rangle.$$

After the second step, the state is

$$\sum_{\tilde{h}(q)=j} \hat{f}[d(q)] |q_{L-1}\dots q_j\rangle |\tilde{d}(q_{j-1}\dots q_0, j, q_j)\rangle |1\dots 10\dots 0\rangle.$$

Steps 3-4 apply QFT of j -qubits to the state, which results in

$$\sum_{\tilde{h}(q)=j} |q_{L-1}\dots q_j\rangle \left(2^{-j/2} \sum_{n=0}^{2^j-1} \hat{f}[d(q)] e^{i2^{-j}n \cdot \tilde{d}(q_{j-1}\dots q_0, j, q_j)} |n\rangle \right) |1\dots 10\dots 0\rangle.$$

After the last step

$$\sum_{\tilde{h}(q)=j} |q_{L-1} \dots q_{j+1}\rangle \left(2^{-j/2} \sum_{n=0}^{2^j-1} \hat{f}[d(q)] e^{\mathbf{i}2\pi 2^{-j} n \cdot \tilde{d}(q_{j-1} \dots q_0, j, q_j)} |n\rangle \right) |0\rangle = (\star_1)$$

if we denote $q_{L-1} \dots q_j$ as m , and $q_{j-1} \dots q_0$ as \tilde{q} then

$$(\star_1) = \sum_{m \text{ s.t. } W_m^j \in \Lambda_T} |m\rangle \sum_{\tilde{q}=0}^{2^j-1} \left(2^{-j/2} \sum_{n=0}^{2^j-1} \hat{f}[d(m2^j + \tilde{q})] e^{\mathbf{i}2\pi 2^{-j} n \cdot \tilde{d}(\tilde{q}, j, q_{j+1})} |n\rangle \right) |0\rangle = (\star_2)$$

However, for fixed j and n , $\tilde{d}(\tilde{q}, j, q_j) = d(m2^j + \tilde{q})$, and given the support of $\hat{\varphi}_{m,n}^j$,

$$\begin{aligned} \sum_{q=0}^{2^L-1} \overline{\hat{\varphi}_{m,n}^j(d(q))} \hat{f}[d(q)] &= \sum_{\tilde{q}=0}^{2^j-1} \overline{\hat{\varphi}_{m,n}^j(2\pi d(m2^j + \tilde{q}))} \hat{f}[d(m2^j + \tilde{q})] \\ &= 2^{-j/2} \sum_{\tilde{q}=0}^{2^j-1} \hat{f}[d(m2^j + \tilde{q})] e^{\mathbf{i}2\pi 2^{-j} n \cdot \tilde{d}(\tilde{q}, j, q_{j+1})} \end{aligned}$$

Together,

$$(\star_2) = \sum_{m \text{ s.t. } W_m^j \in \Lambda_T} \sum_{n=0}^{2^j-1} \left(\sum_{q=0}^{2^L-1} \overline{\hat{\varphi}_{m,n}^j(d(q))} \hat{f}[d(q)] \right) |m2^j + n\rangle.$$

The sum over all possible j 's gives the evolution claimed by the algorithm. \square

A.2 Wave atoms

Algorithm 5 Quantum wave atoms: Operation F^A (see Section 5.4)

Input: $|\hat{f}\rangle = \sum_{q=0}^{2^L-1} \hat{f}[d(q)] |q\rangle$.

Result: $|f^D\rangle = \sum_{W_m^j \in \Lambda_T} \sum_{n=0}^{2^j-1} \left(\sum_{q=0}^{2^L-1} F_{m2^j+n,q}^A \hat{f}[d(q)] \right) |m2^j + n\rangle$.

Notation:

- Quantum register \mathcal{R}_q of L qubits contains the input state; $\mathcal{R}_q[i]$ corresponds to i -th qubit in register \mathcal{R}_q , $i = 0, \dots, L-1$;
- Quantum register \mathcal{R}_h of $L-1$ qubits contains ancilla qubits in zero initial state with indices starting from 1, i.e. $\mathcal{R}_h[i]$ is initialized in the state $|0\rangle$, $i = 1, \dots, L-1$.

1. Apply gate R_0 to qubit $\mathcal{R}_q[0]$.
2. Compute h_j , $1 \leq j < L$, by calling subroutines such that for basis state $|q\rangle$

$$\underbrace{|q\rangle}_{\mathcal{R}_q} \underbrace{|0\rangle}_{\mathcal{R}_h} \mapsto |q\rangle |h_1(q)h_2(q) \dots h_{L-1}(q)\rangle,$$

in other words, qubit $\mathcal{R}_h[i]$ is in state $|h_i(q)\rangle$.

3. For each $j = 1, \dots, L-1$ apply $(-iZ)$ -gate to qubit $\mathcal{R}_q[0]$ controlled on $\mathcal{R}_q[j] = |1\rangle$, $\mathcal{R}_h[j] = |1\rangle$ and $\mathcal{R}_h[j+1] = |0\rangle$ (for $j = L-1$, the latter condition is omitted).
 4. For each $j = 1, \dots, L-1$ apply decoding circuit \tilde{D}_j to qubits $\mathcal{R}_q[0], \dots, \mathcal{R}_q[j]$ controlled on $\mathcal{R}_h[j] = |1\rangle$ and $\mathcal{R}_h[j+1] = |0\rangle$ (for $j = L-1$, the latter condition is omitted and \tilde{D}_j is applied to $\mathcal{R}_q[0], \dots, \mathcal{R}_q[j-1]$).
 5. For each $j = 1, \dots, L-1$, and each $i = 0, \dots, j-1$, apply P_{j-i+1} gate to $\mathcal{R}_q[i]$ controlled on $\mathcal{R}_h[j] = |1\rangle$ and $\mathcal{R}_h[j+1] = |0\rangle$.
 6. For each integer j starting from $j = L$ to $j = 1$, apply QFT rotation Q_j^R to qubits $\mathcal{R}_q[0], \dots, \mathcal{R}_q[j-1]$ controlled on qubit $\mathcal{R}_h[j] = |1\rangle$.
 7. For each $j = 2, \dots, L$ apply QFT swap Q_j^S to qubits $\mathcal{R}_q[0], \dots, \mathcal{R}_q[j-1]$ controlled on $\mathcal{R}_h[j] = |1\rangle$ and $\mathcal{R}_h[j+1] = |0\rangle$ (the latter condition is omitted for $j = L-1$).
 8. Undo the computation of step 2, returning the register \mathcal{R}_h to the state $|0\rangle$. This is feasible because the action of steps 3-7 on the register \mathcal{R}_q is block-diagonal, i.e., it preserves each subspace $\text{span}\{|q\rangle \mid \tilde{h}(q) = j\}$.
-

Proof Let's consider the evolution of $|\hat{f}\rangle$ within the subspace $\text{span}\{|q\rangle \mid \tilde{h}(q) = j\}$,

$$\sum_{\tilde{h}(q)=j} \hat{f}[d(q)] |q\rangle |0\rangle = \sum_{\tilde{h}(q)=j} \hat{f}[d(q)] |q_{L-1}\rangle \dots |q_0\rangle |0\rangle.$$

After the first step, the state is

$$\sum_{\tilde{h}(q)=j} (-1)^{q_0} e^{(-1)^{q_0+1} i\pi/4} \hat{f}[d(q)] |q\rangle |0\rangle.$$

After the second step, the state is

$$\sum_{\tilde{h}(q)=j} (-1)^{q_0} e^{(-1)^{q_0+1} i\pi/4} \hat{f}[d(q)] |q\rangle |\underbrace{1 \dots 1}_j 0 \dots\rangle.$$

After the third step, the state is

$$\sum_{\tilde{h}(q)=j} (-1)^{q_0 \vee q_j} \mathbf{i}^{q_j} e^{(-1)^{q_0+1} \mathbf{i} \pi / 4} \hat{f}[d(q)] |q\rangle |1 \dots 10 \dots 0\rangle.$$

After the fourth step, the state is

$$\begin{aligned} & \sum_{\tilde{h}(q)=j} (-1)^{q_0 \vee q_j} \mathbf{i}^{q_j} e^{(-1)^{q_0+1} \mathbf{i} \pi / 4} \hat{f}[d(q)] |q_{L-1}\rangle \dots |q_j\rangle \\ & \otimes |\tilde{d}(q_{j-1} \dots q_0, k, q_j)\rangle |1 \dots 10 \dots 0\rangle. \end{aligned}$$

After the fifth step, the state is

$$\begin{aligned} & \sum_{\tilde{h}(q)=j} (-1)^{q_0 \vee q_j} \mathbf{i}^{q_j} e^{(-1)^{q_0+1} \mathbf{i} \pi / 4} \hat{f}[d(q)] |q_{L-1}\rangle \dots |q_j\rangle \\ & \otimes e^{\mathbf{i} \pi 2^{-j} \tilde{d}(q_{j-1} \dots q_0, k, q_j)} |\tilde{d}(q_{j-1} \dots q_0, k, q_j)\rangle |1 \dots 10 \dots 0\rangle, \end{aligned}$$

After the steps 6 – 8, the state is

$$\begin{aligned} & \sum_{\tilde{h}(q)=j} (-1)^{q_0 \vee q_j} \mathbf{i}^{q_j} e^{(-1)^{q_0+1} \mathbf{i} \pi / 4} \hat{f}[d(q)] |q_{L-1}\rangle \dots |q_j\rangle \\ & \otimes e^{\mathbf{i} \pi 2^{-j} \tilde{d}(q_{j-1} \dots q_0, k, q_j)} \left(2^{-j/2} \sum_{n=0}^{2^j-1} e^{\mathbf{i} 2^{-j} n \cdot \tilde{d}(q_{j-1} \dots q_0, j, q_j)} |n\rangle \right) |0\rangle, \end{aligned}$$

if we denote $q_{L-1} \dots q_j$ as m , and $q_{j-1} \dots q_0$ as \tilde{q} then we can re-write the final state as

$$(\star_1) = \sum_{m \text{ s.t. } W_m^j \in \Lambda_T} \sum_{n=0}^{2^j-1} \sum_{\tilde{q}=0}^{2^j-1} F_{m2^j+n, m2^j+\tilde{q}}^A \hat{f}[d(m2^j + \tilde{q})] |m2^j + n\rangle |0\rangle = (\star)$$

However, $F_{m2^j+n, q}^A = 0$ for $q \notin \{m2^j, \dots, (m+1)2^j - 1\}$, so

$$(\star) = \sum_{m \text{ s.t. } W_m^j \in \Lambda_T} \sum_{n=0}^{2^j-1} \sum_{q=0}^{2^L-1} F_{m2^j+n, q}^A \hat{f}[d(q)] |m2^j + n\rangle |0\rangle.$$

The sum over all possible j 's gives the evolution claimed by the algorithm. \square

Algorithm 6 Operation \tilde{G}^A , using linear Pauli rotations (see Section 5.5.1)

Input:

$$|\alpha\rangle = \sum_{W_m^j \in \Lambda_T} \sum_{n=0}^{2^{j-1}-1} |m2^{j-1} + n\rangle (\alpha_{m2^j+2n} |0\rangle + \alpha_{m2^j+2n+1} |1\rangle)$$

Output:

$$\begin{aligned} \tilde{G}^A |\alpha\rangle = & \sum_{W_m^j \in \Lambda_T} \sum_{n=0}^{2^{j-1}-1} |m2^{j-1} + n\rangle \otimes \\ & \left(\begin{pmatrix} \cos(v(j, m, n)) & i \sin(v(j, m, n)) \\ i \sin(v(j, m, n)) & \cos(v(j, m, n)) \end{pmatrix} (\alpha_{m2^j+2n} |0\rangle + \alpha_{m2^j+2n+1} |1\rangle) \right). \end{aligned}$$

Notation:

- Quantum register \mathcal{R}_q of L qubits contains the input state; $\mathcal{R}_q[i]$ corresponds to i -th qubit in register \mathcal{R}_q , $i = 0, \dots, L-1$
- Quantum register \mathcal{R}_h of $L-1$ qubits contains ancilla qubits in zero initial state with indices starting from 1, i.e., $\mathcal{R}_h[i]$ is initialized in the state $|0\rangle$, $i = 1, \dots, L-1$
- Quantum register \mathcal{R}_I of 1 qubit contains an ancilla qubit in zero initial state.

1. Apply S -gate to $\mathcal{R}_q[0]$.
2. Compute h_j , $1 \leq j < L$, by calling subroutines such that for basis state $|q\rangle$

$$\underbrace{|q\rangle}_{\mathcal{R}_q} \underbrace{|0\rangle}_{\mathcal{R}_h} \underbrace{|0\rangle}_{\mathcal{R}_I} \mapsto |q\rangle |h_1(q) \dots h_{L-1}(q)\rangle |0\rangle,$$

in other words, qubit $\mathcal{R}_h[i]$ is in the state $|h_i(q)\rangle$.

3. For each $j = 1, \dots, L-1$ controlled on $\mathcal{R}_h[j] = |1\rangle$, $\mathcal{R}_h[j+1] = |0\rangle$:
 - (a) Compute Comparator $_{j-1}(\mu_0(j, 0)+1)$ applied to qubits $\mathcal{R}_q[1], \dots, \mathcal{R}_q[j-1]$ with the result added to \mathcal{R}_I ancilla qubit.
 - (b) Apply linear Pauli rotation (see Figure 12) with slope of $3\pi 2^{-j}$ and offset of $-\pi$ controlled on $\mathcal{R}_I = |1\rangle$ and $\mathcal{R}_q[j] = |0\rangle$.
 - (c) Apply linear Pauli rotation with slope of $3\pi 2^{-(j+1)}$ and offset of $-\frac{\pi}{2}$ controlled on $\mathcal{R}_I = |0\rangle$ and $\mathcal{R}_q[j] = |0\rangle$.
 - (d) Undo the computation of step 3a, returning the register \mathcal{R}_I to the state $|0\rangle$. This is feasible because steps 3b-3c are limited to action on qubit $\mathcal{R}_q[0]$.
 - (e) Compute Comparator $_{j-1}(\mu_0(j, 1)+1)$ applied to qubits $\mathcal{R}_q[1], \dots, \mathcal{R}_q[j-1]$ with the result added to \mathcal{R}_I ancilla qubit.
 - (f) Apply linear Pauli rotation with slope of $3\pi 2^{-(j+1)}$ and offset of $-\frac{\pi}{4}$ controlled on $\mathcal{R}_I = |1\rangle$ and $\mathcal{R}_q[j] = |1\rangle$.
 - (g) Apply linear Pauli rotation with slope of $3\pi 2^{-j}$ and offset of $-\frac{\pi}{2}$ controlled on that $\mathcal{R}_I = |0\rangle$ and $\mathcal{R}_q[j] = |1\rangle$.
 - (h) Undo the computation of step 3e, returning the register \mathcal{R}_I to the state $|0\rangle$. This is feasible because steps 3f-3g are limited to action on qubit $\mathcal{R}_q[0]$.
4. Undo the computation of step 2, returning the register \mathcal{R}_h to the state $|0\rangle$. This is feasible because the action of step 3 on the register \mathcal{R}_q is block-diagonal, i.e., it preserves each subspace $\text{span}\{|q\rangle \mid \tilde{h}(q) = j\}$.
5. Apply inverse S -gate to $\mathcal{R}_q[0]$.

Proof For the proof, let us denote

$$R(\theta) = \begin{pmatrix} \cos(\theta) & \sin(\theta) \\ -\sin(\theta) & \cos(\theta) \end{pmatrix}.$$

Let's consider the evolution within the subspace $\text{span}\{|q\rangle \mid \tilde{h}(q) = j\}$ for a fixed j , in other words,

$$\sum_{m \text{ s.t. } W_m^j \in \Lambda_T} \sum_{n=0}^{2^{j-1}-1} |m2^{j-1} + n\rangle (\alpha_{m2^j+2n} |0\rangle + \alpha_{m2^j+2n+1} |1\rangle) |0\rangle |0\rangle.$$

After the first step, the state is

$$\sum_{m \text{ s.t. } W_m^j \in \Lambda_T} \sum_{n=0}^{2^{j-1}-1} |m2^{j-1} + n\rangle (\alpha_{m2^j+2n} |0\rangle + \mathbf{i}\alpha_{m2^j+2n+1} |1\rangle) |0\rangle |0\rangle.$$

After the second step, the state is

$$\sum_{m \text{ s.t. } W_m^j \in \Lambda_T} \sum_{n=0}^{2^{j-1}-1} |m2^{j-1} + n\rangle (\alpha_{m2^j+2n} |0\rangle + \mathbf{i}\alpha_{m2^j+2n+1} |1\rangle) |\underbrace{1 \dots 1}_j 0 \dots 0\rangle |0\rangle.$$

After step 3a, the state is

$$\sum_{m \text{ s.t. } W_m^j \in \Lambda_T} \sum_{n=0}^{2^{j-1}-1} |m2^{j-1} + n\rangle (\alpha_{m2^j+2n} |0\rangle + \mathbf{i}\alpha_{m2^j+2n+1} |1\rangle) |1 \dots 10 \dots 0\rangle \otimes |I(n \geq \mu_0(j, 0) + 1)\rangle.$$

Note that $I(n \geq \mu_0(j, 0) + 1) = I(n > 2^j/3)$ as $n, j \in \mathbb{Z}$. After step 3b, the state is

$$\sum_{m \text{ s.t. } W_m^j \in \Lambda_T} \sum_{n=0}^{2^{j-1}-1} (|m2^{j-1} + n\rangle \otimes \left(R\left(\frac{\pi}{2^{j+1}}(3n - 2^j)I(m \text{ is even})I(n > 2^j/3)\right) (\alpha_{m2^j+2n} |0\rangle + \mathbf{i}\alpha_{m2^j+2n+1} |1\rangle) \right) \otimes |1 \dots 10 \dots 0\rangle |I(q_{j-1} \dots q_1 \geq \mu_0(j, 0) + 1)\rangle).$$

After step 3c, the state is

$$\sum_{m \text{ s.t. } W_m^j \in \Lambda_T} \sum_{n=0}^{2^{j-1}-1} (|m2^{j-1} + n\rangle \otimes \left(R\left(\frac{2^{I(n > 2^j/3)}\pi}{2^{j+1}}(3n - 2^j)I(m \text{ is even})\right) (\alpha_{m2^j+2n} |0\rangle + \mathbf{i}\alpha_{m2^j+2n+1} |1\rangle) \right) \otimes |1 \dots 10 \dots 0\rangle |I(q_{j-1} \dots q_1 \geq \mu_0(j, 0) + 1)\rangle).$$

After step 3d, the state is

$$\sum_{m \text{ s.t. } W_m^j \in \Lambda_T} \sum_{n=0}^{2^{j-1}-1} (|m2^{j-1} + n\rangle \otimes \left(R\left(\frac{2^{I(n > 2^j/3)}\pi}{2^{j+1}}(3n - 2^j)I(m \text{ is even})\right) (\alpha_{m2^j+2n} |0\rangle + \mathbf{i}\alpha_{m2^j+2n+1} |1\rangle) \right) \otimes |1 \dots 10 \dots 0\rangle |I(q_{j-1} \dots q_1 \geq \mu_0(j, 0) + 1)\rangle).$$

$$\otimes |1 \dots 10 \dots 0\rangle |0\rangle \Big).$$

Steps 3a-3d actions are limited to even m 's. Steps 3e-3h are similar but applied to odd m 's. At the end of step 3, the state is

$$\begin{aligned} & \sum_{m \text{ s.t. } W_m^j \in \Lambda_T} \sum_{n=0}^{2^{j-1}-1} (|m2^{j-1} + n\rangle \\ & \otimes \left(R \left(\frac{2^{I(n > 2^{j/3})} \pi}{2^{j+1}} (3n - 2^j) I(m \text{ is even}) \right) R \left(\frac{2^{I(n < 2^{j-1}/3)} \pi}{2^{j+2}} (3n - 2^{j-1}) I(m \text{ is odd}) \right) \right. \\ & \quad \left. (\alpha_{m2^j+2n} |0\rangle + \mathbf{i} \alpha_{m2^j+2n+1} |1\rangle) \right) \\ & \otimes |1 \dots 10 \dots 0\rangle |0\rangle \Big), \end{aligned}$$

with the use of function $v(\cdot)$ we can re-write the state as

$$\sum_{m \text{ s.t. } W_m^j \in \Lambda_T} \sum_{n=0}^{2^{j-1}-1} |m2^{j-1} + n\rangle \otimes R(v(j, m, n)) (\alpha_{m2^j+2n} |0\rangle + \mathbf{i} \alpha_{m2^j+2n+1} |1\rangle) \otimes |1 \dots 10 \dots 0\rangle |0\rangle.$$

After the fourth step, the state is

$$\sum_{m \text{ s.t. } W_m^j \in \Lambda_T} \sum_{n=0}^{2^{j-1}-1} |m2^{j-1} + n\rangle \otimes R(v(j, m, n)) (\alpha_{m2^j+2n} |0\rangle + \mathbf{i} \alpha_{m2^j+2n+1} |1\rangle) \otimes |0\rangle |0\rangle.$$

As

$$\alpha_{m2^j+2n} |0\rangle + \mathbf{i} \alpha_{m2^j+2n+1} |1\rangle = S(\alpha_{m2^j+2n} |0\rangle + \alpha_{m2^j+2n+1} |1\rangle),$$

the final state is

$$\sum_{m \text{ s.t. } W_m^j \in \Lambda_T} \sum_{n=0}^{2^{j-1}-1} |m2^{j-1} + n\rangle \otimes R^{(i)}(v(j, m, n)) (\alpha_{m2^j+2n} |0\rangle + \alpha_{m2^j+2n+1} |1\rangle) \otimes |0\rangle |0\rangle,$$

where

$$R^{(i)}(\theta) = \begin{pmatrix} \cos(\theta) & \mathbf{i} \sin(\theta) \\ \mathbf{i} \sin(\theta) & \cos(\theta) \end{pmatrix}.$$

□

Algorithm 7 Computing the functions $h_j^\rho(\cdot)$ (see Section 5.6)

Input: $|\alpha\rangle |0\rangle |0\rangle |0\rangle = \sum_{q=0}^{2^{L-1}-1} \alpha_q |q\rangle |0\rangle |0\rangle |0\rangle$.

Result: $\sum_{q=0}^{2^{L-1}-1} \alpha_q |q\rangle |h_1^\rho(q), \dots, h_{L-2}^\rho(q)\rangle |0\rangle |0\rangle$.

Notation:

Quantum register \mathcal{R}_q of $L-1$ qubits containing the input state $|\alpha\rangle$; $\mathcal{R}_q[i]$ corresponds to i -th qubit in register \mathcal{R}_q , $i = 0, \dots, L-2$;

Quantum register \mathcal{R}'_h of $L-1$ qubits in initial state $|0\rangle$; $\mathcal{R}'_h[i]$ corresponds to i -th qubit in register \mathcal{R}'_h , $i = 1, \dots, L-1$;

Quantum register \mathcal{R}_h of $L-1$ ancilla qubits in initial state $|0\rangle$; $\mathcal{R}_h[i]$ corresponds to i -th qubit in register \mathcal{R}_h , $i = 1, \dots, L-1$;

Quantum register \mathcal{R}_I of 2 ancilla qubits in initial state $|0\rangle$.

1. Compute h_j , $1 \leq j < L$, by calling subroutines on the register \mathcal{R}_q and ancilla qubit $\mathcal{R}_I[0]$ as the least significant qubit,

$$\underbrace{|q\rangle}_{\mathcal{R}_q} \underbrace{|0\rangle}_{\mathcal{R}'_h} \underbrace{|0\rangle}_{\mathcal{R}_h} \underbrace{|0\rangle}_{\mathcal{R}_I} \mapsto |q\rangle |0\rangle |h_1(q), \dots, h_{L-1}(q)\rangle |0\rangle.$$

2. Apply $\text{Compare}_{L-1}(\mu_0(j, 0) + 1)$ to \mathcal{R}_q with the result added to $\mathcal{R}_I[0]$;
 3. Apply $\text{Compare}_{L-1}(m_r 2^{j_r-1} + \mu_0(j_r, m_r) + 1)$ to \mathcal{R}_q with the result added to $\mathcal{R}_I[0]$;
 4. For each $j = 2, \dots, L-1$ controlled on that $\mathcal{R}_h[j] = |1\rangle$, $\mathcal{R}_h[j+1] = |0\rangle$ and $\mathcal{R}_I[0] = |1\rangle$:
 - (a) Apply $\text{Compare}_j(\mu_0(j, 0) + 1)$ to the first $j-1$ qubits in \mathcal{R}_q controlled on that $\mathcal{R}_q[j-1] = |0\rangle$ and add the result to $\mathcal{R}_I[1]$;
 - (b) Apply $\text{Compare}_j(\mu_0(j, 1) + 1)$ to the first $j-1$ qubits in \mathcal{R}_q controlled on that $\mathcal{R}_q[j-1] = |1\rangle$ and add the result to $\mathcal{R}_I[1]$;
 - (c) Apply X -gate to qubit $\mathcal{R}'_h[j]$ controlled on $\mathcal{R}_I[1] = |0\rangle$ and $\mathcal{R}_q[j-1] = |0\rangle$;
 - (d) Apply X -gate to qubit $\mathcal{R}'_h[j]$ controlled on $\mathcal{R}_I[1] = |1\rangle$ and $\mathcal{R}_q[j-1] = |1\rangle$;
 - (e) Apply X -gate to qubit $\mathcal{R}'_h[j-1]$ controlled on $\mathcal{R}_I[1] = |0\rangle$ and $\mathcal{R}_q[j-1] = |1\rangle$;
 - (f) Apply X -gate to qubit $\mathcal{R}'_h[j-1]$ controlled on $\mathcal{R}_I[1] = |1\rangle$, $\mathcal{R}_q[j-1] = |0\rangle$;
 - (g) Un-compute steps (b) and (a).
 5. Un-compute steps 3, 2, 1.
-

Proof Here $\mathcal{R}_I[0] = |1\rangle$ allows us to avoid permuting the border cases and computed in steps 2-3. $\mathcal{R}_I[1] = |1\rangle$ computed in step 4a-4b controls the condition $n > \mu(j, m)$. This condition depends on the parity of m which is equal to $\mathcal{R}_q[j-1]$. Finally, steps 4c-4f implement the logic outlined in the main text. \square

Appendix B Proofs

B.1 Section 2.3: Wavelet packet trees

Proof of Proposition 1: We traverse the tree as follows:

1. We start from the root node W_0^L and descend the tree while always moving down to a left child, so at each level $W_0^j \mapsto W_0^{j-1}$. Suppose that we stopped at node $W_0^{j'}$, then $W_0^{j'}$ is a leaf node; otherwise, it should have left and right children. Therefore, the first node in the traverse is $W_0^{j'}$, i.e. $m_1 = 0$.
2. Imagine that we will add nodes to the tree T until it becomes a perfect binary tree of height of L , that is, for each leaf node W_m^j we append a perfect binary subtree of height j at that node. Then the leftmost leaf node in the subtree with root W_m^j is $W_{m_i 2^{j_i}}^0$, and the rightmost leaf node is $W_{m'}^0$ where $m' = (m_i + 1)2^{j_i} - 1$. The leaf node next to $W_{m'}^0$ is the leftmost leaf node in the subtree with root $W_{m_{i+1}}^{j_{i+1}}$, which is $W_{m_{i+1} 2^{j_{i+1}}}^0$. Therefore, $(m_i + 1)2^{j_i} = m_{i+1} 2^{j_{i+1}}$.
3. Observe that the rightmost node in the expanded perfect binary tree (constructed in 2) is $W_{2^L - 1}^0$ and is also the rightmost node of the subtree with root $W_{m_K}^{j_K}$. Therefore, $(m_K + 1)2^{j_K} = 2^L$.

□

B.2 Section 3.1.2: Retaining decoding circuit

Proof of correctness of circuit \tilde{D}_j (Algorithm 2):

Recall the definition of \tilde{d} in equation 21 and write it in terms of q

$$\tilde{d}(q, j, m) = \begin{cases} 2^{j-1} \cdot I(m \text{ is odd}) + \frac{q}{2}, & \text{if } q \text{ is even,} \\ 2^j - 2^{j-1} \cdot I(m \text{ is odd}) - \frac{q+1}{2}, & \text{if } q \text{ is odd.} \end{cases}$$

In binary representation $q = q_{j-1}, q_{j-2}, \dots, q_0$. For even q ($q_0 = 0$),

$$q/2 = 0, q_{j-1}, \dots, q_1.$$

For odd q ($q_0 = 1$),

$$2^j - (q + 1)/2 = 1, (q_{j-1} \oplus 1), \dots, (q_1 \oplus 1).$$

Combined:

$$\tilde{d}(q, j, m) = \tilde{d}(q_{j-1}, q_{j-2}, \dots, q_0; j; m) = (q_0 \oplus m), (q_{j-1} \oplus q_0), \dots, (q_1 \oplus q_0).$$

The description of the algorithm has the evolution of each basis state. The final state is

$$\sum_{q=0}^{2^j-1} \alpha_q |m\rangle |q_0 \oplus m\rangle |q_{j-1} \oplus q_0\rangle \dots |q_1 \oplus q_0\rangle = \sum_{q=0}^{2^j-1} \alpha_q |m\rangle |\tilde{d}(q, j, m)\rangle. \quad \square$$

B.3 Section 5.1: Wave atoms' support over the frequency domain

Proof of Proposition 3:

Given that the support is symmetric around zero. Without loss of generality, we consider only the non-negative frequencies. For odd m , the support of $\hat{\psi}_m^j$ is

$$\left(2^{j-1}(m - \frac{1}{3}), 2^{j-1}(m + 1 + \frac{2}{3})\right)$$

$$= \left(2^{j-1}(m - \frac{1}{3}), 2^{j-1}(m + \frac{1}{3})\right) \cup \{2^{j-1}(m + \frac{1}{3})\} \cup \left(2^{j-1}(m + 1 - \frac{2}{3}), 2^{j-1}(m + 1 + \frac{2}{3})\right).$$

Given that $2^{j-1}(m + \frac{1}{3})$ is never an integer, we can ignore this point. Further, as $2^{j-1}m$ and $2^{j-1}(m + 1)$ are integers, the integer support of $\hat{\psi}_m^j$ becomes

$$\left[2^{j-1}m - \lfloor 2^{j-1}/3 \rfloor, 2^{j-1}m + \lfloor 2^{j-1}/3 \rfloor\right] \cup \left[2^{j-1}(m + 1) - \lfloor 2^j/3 \rfloor, 2^{j-1}(m + 1) + \lfloor 2^j/3 \rfloor\right].$$

Given that for odd m , $\mu_0(j, m) = \lfloor 2^{j-1}/3 \rfloor$ and $\mu_1(j, m) = \lfloor 2^j/3 \rfloor$, this concludes the proof for the case of odd m . Similarly for even m . \square

B.4 Section 5.3: Decomposition of C^A

We state two identities due to periodicity of the complex exponential function and the definition of $\alpha_m = \frac{\pi}{2}(m + \frac{1}{2})$:

$$e^{\mathbf{i}2\pi 2^{-j}(n+\frac{1}{2})(-m2^{j-1}+s)} e^{\mathbf{i}\alpha_m} = \mathbf{i} e^{\mathbf{i}2\pi 2^{-j}(n+\frac{1}{2})(m2^{j-1}+s)} e^{-\mathbf{i}\alpha_m} \quad (\text{B1})$$

$$e^{\mathbf{i}2\pi 2^{-j}(n+\frac{1}{2})((m+1)2^{j-1}+s)} e^{-\mathbf{i}\alpha_m} = \mathbf{i} e^{\mathbf{i}2\pi 2^{-j}(n+\frac{1}{2})(-(m+1)2^{j-1}+s)} e^{\mathbf{i}\alpha_m} \quad (\text{B2})$$

Also we state a simple identity:

$$g((-1)^m(2^{-j+1}\pi(-s) - \frac{\pi}{2})) = g((-1)^{m+1}(2^{-j+1}\pi s + \frac{\pi}{2})) \quad (\text{B3})$$

Our goal is to implement the operation described in Definition 4:

$$\sum_{i=0}^{N-1} C_{m2^j+n,i}^A \hat{f}[d(i)] = \sum_{i=0}^{N-1} \overline{\hat{\psi}_{m,n}^j(d(i))} \hat{f}[d(i)]. \quad (\text{B4})$$

Recall that $\tilde{\psi}_m^j$ is related to $\hat{\psi}_m^j$ via equations (35)-(36), and $\hat{\psi}_m^j$ is supported on two intervals in the frequency domain, described by equation (30) and proposition 3. This motivates us to state and prove the following two lemmas.

Lemma 1. For any $W_m^j \neq W_0^j$,

$$\begin{aligned} \sum_{|s| \leq \mu_0(j,m)} \left(\overline{\hat{\psi}_{m,n}^j(m2^{j-1}+s)} \hat{f}[m2^{j-1}+s] + \overline{\hat{\psi}_{m,n}^j(-m2^{j-1}+s)} \hat{f}[-m2^{j-1}+s] \right) \\ = \sum_{i_k=m2^j}^{m2^j+2\mu_0(j,m)} F_{m2^j+n,i_k}^A \sum_{c=0}^{N-1} G_{\rho(i_k),c}^A \hat{f}[d(\rho(c))]. \end{aligned} \quad (\text{B5})$$

Proof For $s \geq 0$ we use identity (B1) for points on negative side.

$$\begin{aligned} \overline{\hat{\psi}_{m,n}^j(m2^{j-1}+s)} &= 2^{-j/2} e^{\mathbf{i}2\pi 2^{-j}(n+\frac{1}{2})(m2^{j-1}+s)} e^{-\mathbf{i}\alpha_m} g((-1)^m(2^{-j+1}\pi|s| - \frac{\pi}{2})) \\ &= F_{m2^j+n,m2^j+2s}^A G_{\rho(m2^j+2s),m2^j+2s}^A, \\ \overline{\hat{\psi}_{m,n}^j(-m2^{j-1}+s)} &= 2^{-j/2} e^{\mathbf{i}2\pi 2^{-j}(n+\frac{1}{2})(m2^{j-1}+s)} e^{-\mathbf{i}\alpha_m} \mathbf{i} g((-1)^{m+1}(2^{-j+1}\pi|s| + \frac{\pi}{2})) \\ &= F_{m2^j+n,m2^j+2s}^A G_{\rho(m2^j+2s),m2^j+2s-1}^A. \end{aligned}$$

For $s < 0$ we use the identity (B1) for points on positive side. Moreover, we use the identity (B3) for points on both sides.

$$\begin{aligned}
\overline{\hat{\psi}_{m,n}^j(m2^{j-1} + s)} &= 2^{-j/2} e^{i2\pi 2^{-j}(n+\frac{1}{2})(-m2^{j-1}+s)} e^{i\alpha_m} (-i) g((-1)^{m+1} (2^{-j+1} \pi |s| + \frac{\pi}{2})) \\
&= F_{m2^j+n, m2^j+2|s|-1}^A G_{\rho(m2^j+2|s|-1), m2^j-2|s|}^A, \\
\overline{\hat{\psi}_{m,n}^j(-m2^{j-1} + s)} &= 2^{-j/2} e^{i2\pi 2^{-j}(n+\frac{1}{2})(-m2^{j-1}+s)} e^{i\alpha_m} g((-1)^m (2^{-j+1} \pi |s| - \frac{\pi}{2})) \\
&= F_{m2^j+n, m2^j+2|s|-1}^A G_{\rho(m2^j+2|s|-1), m2^j-2|s|-1}^A.
\end{aligned}$$

Therefore, the left-hand side of equation (B5) becomes

$$\begin{aligned}
&\sum_{|s| \leq \mu_0(j,m)} \left(\overline{\hat{\psi}_{m,n}^j(m2^{j-1} + s)} \hat{f}[m2^{j-1} + s] + \overline{\hat{\psi}_{m,n}^j(-m2^{j-1} + s)} \hat{f}[-m2^{j-1} + s] \right) \\
&= \sum_{s=0}^{\mu_0(j,m)} F_{m2^j+n, m2^j+2s}^A \left(G_{\rho(m2^j+2s), m2^j+s}^A \hat{f}[d(\rho(m2^j + 2s))] \right. \\
&\quad \left. + G_{\rho(m2^j+2s), m2^j+2s-1}^A \hat{f}[d(\rho(m2^j + 2s - 1))] \right) \\
&+ \sum_{s=1}^{\mu_0(j,m)} F_{m2^j+n, m2^j+2|s|-1}^A \left(G_{\rho(m2^j+2|s|-1), m2^j-2|s|}^A \hat{f}[d(\rho(m2^j - 2|s|))] \right. \\
&\quad \left. + G_{\rho(m2^j+2|s|-1), m2^j-2|s|-1}^A \hat{f}[d(\rho(m2^j - 2|s| - 1))] \right) \\
&= \sum_{s=0}^{2\mu_0(j,m)} F_{m2^j+n, m2^j+s}^A \sum_{c=0} G_{\rho(m2^j+s), c}^A \hat{f}[d(\rho(c))].
\end{aligned}$$

The latter step is due to the block diagonal structure of matrix G^A with blocks of size 2×2 . \square

Lemma 2. For any $W_m^j \neq W_{m_r}^{j_r}$,

$$\begin{aligned}
&\sum_{|s| \leq \mu_1(j,m)} \left(\overline{\hat{\psi}_{m,n}^j((m+1)2^{j-1} + s)} \hat{f}[(m+1)2^{j-1} + s] \right. \\
&\quad \left. + \overline{\hat{\psi}_{m,n}^j(-(m+1)2^{j-1} + s)} \hat{f}[-(m+1)2^{j-1} + s] \right) \\
&= \sum_{i_k=m2^j+2\mu_0(j,m)+1}^{(m+1)2^j-1} F_{m2^j+n, i_k}^A \sum_{c=0}^{N-1} G_{\rho(i_k), c}^A \hat{f}[d(\rho(c))].
\end{aligned} \tag{B6}$$

Proof Before reviewing the sum, we show that for any $W_m^j \neq W_{m_r}^{j_r}$ and $s \in \mathbb{Z}$ such that $|s| \leq \mu_1(j, m)$

$$\begin{aligned}
&\begin{pmatrix} G_{(m+1)2^j+2s-1, (m+1)2^j+2s-1}^A & G_{(m+1)2^j+2s-1, (m+1)2^j+2s}^A \\ G_{(m+1)2^j+2s, (m+1)2^j+2s-1}^A & G_{(m+1)2^j+2s, (m+1)2^j+2s}^A \end{pmatrix} \\
&= \begin{pmatrix} g_-[j, m+1, s] & g_+[j, m+1, s] \\ g_+[j, m+1, s] & g_-[j, m+1, s] \end{pmatrix}.
\end{aligned} \tag{B7}$$

Denote the right neighbor of W_m^j by $W_{m'}^{j'}$, then

- If $j' = j$, then $m' = m+1$ and (B7) is simply the definition the block of matrix G^A ;

- If $j' = j + 1$, then both m and m' are odd and by properties of the function g .

$$\begin{aligned} g((-1)^{m'}(2^{-j'+1}\pi s - \frac{\pi}{2})) &= g(-2^{-j'+1}\pi s + \frac{\pi}{2}) \\ &= g(-\frac{\pi}{2} + 2^{-j+1}\pi s) = g((-1)^{m+1}(2^{-j+1}\pi s - \frac{\pi}{2})), \end{aligned} \quad (\text{B8})$$

and

$$\begin{aligned} g((-1)^{m'+1}(2^{-j'+1}\pi s + \frac{\pi}{2})) &= g(2^{-j'+1}\pi s + \frac{\pi}{2}) \\ &= g(-\frac{\pi}{2} - 2^{-j+1}\pi s) = g((-1)^m(2^{-j+1}\pi s + \frac{\pi}{2})). \end{aligned} \quad (\text{B9})$$

- For $j' = j - 1$, then m and m' are even and the derivation is analogous to case of $j' = j + 1$.

For $s \geq 0$ we use the identity (B2) for points on the positive side.

$$\begin{aligned} &\overline{\hat{\psi}_{m,n}^j((m+1)2^{j-1} + s)} \\ &= 2^{-j/2} e^{i2\pi 2^{-j}(n+\frac{1}{2})(-(m+1)2^{j-1}+s)} e^{i\alpha_m} \mathbf{i} g((-1)^m(2^{-j+1}\pi|s| + \frac{\pi}{2})) \\ &= F_{m2^j+n, (m+1)2^j-2s-1}^A G_{\rho((m+1)2^j-2s-1), (m+1)2^j+2s}^A \\ &\quad \overline{\hat{\psi}_{m,n}^j(-(m+1)2^{j-1} + s)} \\ &= 2^{-j/2} e^{i2\pi 2^{-j}(n+\frac{1}{2})(-(m+1)2^{j-1}+s)} e^{i\alpha_m} g((-1)^{m+1}(2^{-j+1}\pi|s| - \frac{\pi}{2})) \\ &= F_{m2^j+n, (m+1)2^j-2s-1}^A G_{\rho((m+1)2^j-2s-1), (m+1)2^j+2s-1}^A. \end{aligned}$$

For $s < 0$ we use the identity (B2) for points on the negative side. Moreover, we use the identity (B3) for points on both sides.

$$\begin{aligned} &\overline{\hat{\psi}_{m,n}^j((m+1)2^{j-1} + s)} \\ &= 2^{-j/2} e^{i2\pi 2^{-j}(n+\frac{1}{2})((m+1)2^{j-1}+s)} e^{-i\alpha_m} g((-1)^{m+1}(2^{-j+1}\pi|s| - \frac{\pi}{2})) \\ &= F_{m2^j+n, (m+1)2^j-2|s|}^A G_{\rho((m+1)2^j-2|s|), (m+1)2^j-2|s|}^A \\ &\quad \overline{\hat{\psi}_{m,n}^j(-(m+1)2^{j-1} + s)} \\ &= 2^{-j/2} e^{i2\pi 2^{-j}(n+\frac{1}{2})((m+1)2^{j-1}+s)} e^{-i\alpha_m} (-\mathbf{i}) g((-1)^m(2^{-j+1}\pi|s| + \frac{\pi}{2})) \\ &= F_{m2^j+n, (m+1)2^j-2|s|}^A G_{\rho((m+1)2^j-2|s|), (m+1)2^j-2|s|-1}^A. \end{aligned}$$

Therefore, the left-hand side of equation (B6) becomes

$$\begin{aligned} &\sum_{|s| \leq \mu_1(j,m)} \left(\overline{\hat{\psi}_{m,n}^j((m+1)2^{j-1} + s)} \hat{f}[(m+1)2^{j-1} + s] \right. \\ &\quad \left. + \overline{\hat{\psi}_{m,n}^j(-(m+1)2^{j-1} + s)} \hat{f}[-(m+1)2^{j-1} + s] \right) \\ &= \sum_{s=0}^{\mu_1(j,m)} F_{m2^j+n, (m+1)2^j-2s-1}^A \times \left(G_{\rho((m+1)2^j-2s-1), (m+1)2^j+2s}^A \hat{f}[d(\rho((m+1)2^j + 2s))] \right. \\ &\quad \left. + G_{\rho((m+1)2^j-2s-1), (m+1)2^j+2s-1}^A \hat{f}[d(\rho((m+1)2^j + 2s-1))] \right) \\ &\quad + \sum_{s=1}^{\mu_1(j,m)} F_{m2^j+n, (m+1)2^j-2s}^A \left(G_{\rho((m+1)2^j-2s), (m+1)2^j-2s}^A \hat{f}[d(\rho((m+1)2^j - 2s))] \right. \\ &\quad \left. + G_{\rho((m+1)2^j-2s), (m+1)2^j-2s-1}^A \hat{f}[d(\rho((m+1)2^j - 2s-1))] \right) \end{aligned}$$

$$= \sum_{s=1}^{2\mu_1(j,m)+1} F_{m2^j+n,(m+1)2^j-s}^A \sum_{c=0}^{N-1} G_{\rho((m+1)2^j-s,c)}^A \hat{f}[d(\rho(c))]$$

The latter step is due to the block diagonal structure of matrix G^A with blocks of size 2×2 . \square

Proof of Theorem 5: First, we consider two special cases. Observe that for $W_0^{j_l}$ and $i_k \leq 2\mu_0(j_l, 0)$ and $n \in \{0, \dots, 2^{j_l} - 1\}$ we have

$$C_{n,i_k}^A = F_{n,i_k}^A \text{ and } R_{i_k,i_k} = G_{i_k,i_k}^A = 1.$$

Also for $W_{m_r}^{j_r}$ and $i_k > m_r 2^{j_r} + 2\mu_0(j_r, m_r)$ and $n \in \{0, \dots, 2^{j_r} - 1\}$ we have

$$C_{m_r 2^{j_r} + n, i_k}^A = F_{m_r 2^{j_r} + n, i_k}^A \text{ and } R_{i_k, i_k} = G_{i_k, i_k}^A = 1.$$

The general case can be handled using lemmas 1 and 2, and proposition 3. Combining all of the above, we get

$$C^A \sum_c^{N-1} \hat{f}[d(c)] |c\rangle = F^A R^\dagger G^A R \sum_c^{N-1} \hat{f}[d(c)] |c\rangle. \quad (\text{B10})$$

Observe that (B10) holds for any \hat{f} and conclude the proof. \square